EVALUATION OF SEGMENTATION

FOR BONE STRUCTURES

IN 3D RENDERING OF

ULTRASOUND RESIDUAL LIMB IMAGES
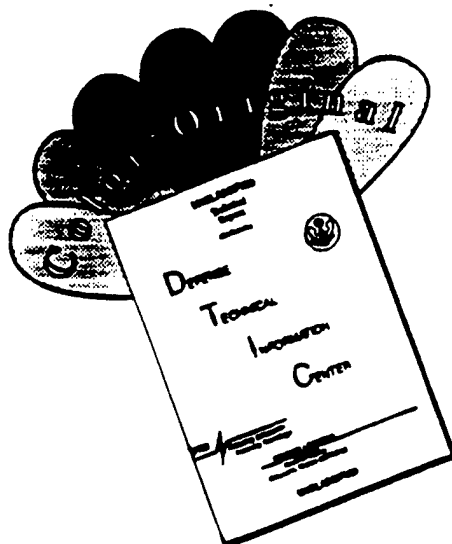
DEPARTMENT OF THE AIR FORCE

AIR UNIVERSITY

AIR FORCE INSTITUTE OF TECHNOLOGY

Wright-Patterson Air Force Base, Ohio

DISCLAIMER NOTICE

THIS DOCUMENT IS BEST
QUALITY AVAILABLE. THE COPY
FURNISHED TO DTIC CONTAINED
A SIGNIFICANT NUMBER OF
COLOR PAGES WHICH DO NOT
REPRODUCE LEGIBLY ON BLACK
AND WHITE MICROFICHE.

EVALUATION OF SEGMENTATION
FOR BONE STRUCTURES
IN 3D RENDERING OF
ULTRASOUND RESIDUAL LIMB IMAGES

THESIS
Min C. Baker
1st Lt, USAF

AFIT/GCS/ENG/96D-03

19970210 031

EVALUATION OF SEGMENTATION FOR BONE STRUCTURES

IN

3D RENDERING OF ULTRASOUND

RESIDUAL LIMB IMAGES

THESIS

Presented to the faculty of the Graduate School of Engineering

of the Air Force Institute of Technology

Air University

In Partial Fulfillment of the

Requirements for the Degree of

Master of Science (Computer Systems)

Min C. Baker, B. S.

1st Lt, USAF

December, 1996

Acknowledgments

Table of Contents

Table of Figures

Abstract

Prosthetists today widely practice manual socket fitting, which produces subjective, inconsistent results. To address this problem, the Computerized Anthropometry Research and Design (CARD) Laboratory is developing a computer-aided socket design system that acquires ultrasound datasets of an amputee's residual limb, creates a 3D model, and helps identify load-bearing and pressure-relief areas. This research project focuses on providing 3D visualization of a residual limb to support the CARD Laboratory's efforts. Creating the 3D model of the skin and two bone contours requires two major steps: segmentation to identify the objects of interest and a surface tracking algorithm to generate the polygonal database of the surface contours. Low-level noise, incomplete boundaries, and widely varying intensities within the images present a difficult challenge to segmentation as well as to the construction of a 3D model. Therefore, different techniques have been explored to achieve accurate segmentation and realistic 3D rendering of unique ultrasound images. Among various segmentation techniques tested, the enhanced 2D multiresolution Bayesian efficiently produces accurate segmentation of outer skin contour and bone locations of the lower limb. The basic technique applies a filter-and-decimate approach coupled with an adaptive clustering algorithm and is modified to use anatomical characteristics to detect and eliminate artifacts.

EVALUATION OF SEGMENTATION

FOR BONE STRUCTURES IN 3D RENDERING OF

ULTRASOUND RESIDUAL LIMB IMAGES

1   *Introduction*

1.1 Background

For various medical reasons, doctors perform approximately 60,000 lower-extremity amputations every year in the United States. For greater mobility, amputees are usually fitted with a prosthesis comprising an artificial foot, shaft, and hand-crafted socket [MORI95].

The pressures of wearing a prosthetic device affect each area of a below-the-knee (BK) amputee's residual limb differently. Because of this uniqueness in response, the prosthetist must decide which areas to load with weight and which areas to relieve from pressure [ENGS92], [SMIT95]. With this concern for comfortably distributing weight and making allowances for sensitive areas, designing a prosthetic socket depends largely on the location of the bone structures in the residual limb. The areas around the tibia, the largest of two bones in the lower leg, tend to bear most of the weight and pressure [MORI95].

With these factors in mind, a prosthetist must customize a socket so that it comfortably fits the contours of an amputee's residual limb while simultaneously providing stable support. Prosthetists perform custom fittings by hand-crafting positive molds of residual limbs to fabricate sockets for a prosthesis [SMIT95]. See Figure 1 for a sketch of a positive mold with built-up relief areas.
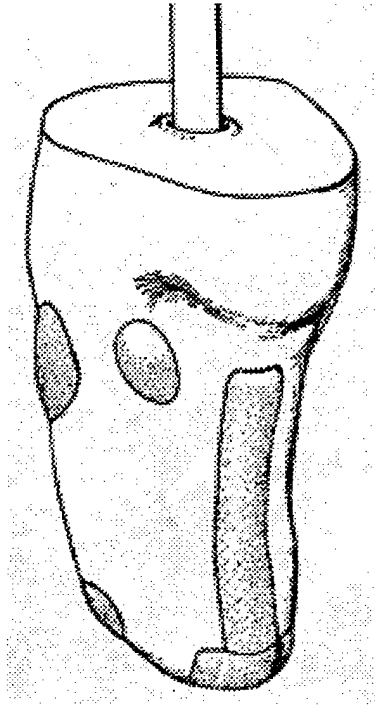
Figure 1 Positive Mold of Residual Limb [SAND86]

Because conventional fitting methods are performed manually, results are subjective, inconsistent, and greatly dependent on the prosthetist [ENGS92], [SMIT95]. Since they rely on the prosthetist's knowledge and experience, these methods also usually require multiple fittings to ensure proper fit of the prosthetic socket. Recurrent fittings make fabrication of the prosthesis very costly. An average prosthesis costs $4,000 and prices can range as high as $15,000 [MORI95].

To reduce fittings and increase comfort, the Computerized Anthropometry Research and Design (CARD) Laboratory at Armstrong Laboratories is developing a computer-aided socket design (CASD) software system that performs socket fittings with higher accuracy than conventional methods, leading to greater cost savings and comfort for amputees [HOUS92]. The CARD Laboratory is also working with Sytronics, Incorporated, Wright State University, and the New York Veterans' Administration (VA) in this endeavor.

1.2 Problem

The CASD software will provide accurate information on the skin contours and bone locations of a BK amputee's residual limb. Three-dimensional (3D) visualization will support the CARD Laboratory's ongoing efforts to create the computer-aided socket design software, which will resolve the problems associated with conventional fitting methods.

My research primarily investigated bone segmentation techniques for 3D visualization of low-noise ultrasound image slices. To obtain lower limb information, the CARD Laboratory chose a specialized ultrasound imaging technique because of its numerous advantages over other types of image acquisition. The technique and its advantages are discussed in Chapter 2.

Because of noise and other problems associated with ultrasound images, my research focused heavily on exploring segmentation techniques for the unique ultrasound images. Segmentation techniques that extract the locations of the bone structures and the outer limb contour are vital for generating accurate lower limb models for the CASD system. My research also provided a means for producing polygonal surface databases of the 3D surface model of the skin and bone contours for use by the CASD system.

1.3 Methodology

Three-dimensional visualization of a residual limb is composed of two major steps: segmentation and 3D rendering. Segmentation separates the objects in a volume dataset that we wish to view [BARI93], [CLAR95], [PAVL82], [SAKA95a], [SAKA95b]. This process is the first operation that needs to be applied to ultrasound image slices. Specifically for this research, the concern is to separate and identify the bone locations from the rest of the limb. Then, the CASD software can display the bones in relation to the limb's surface contours. After completion of segmentation, surface rendering defines surfaces of objects of interest and displays these surfaces using computer graphics techniques [HERM90]. Surface rendering creates a 3D model of the residual limb from the ultrasound dataset.

Many segmentation algorithms already exist for MRI and CT modalities [BEZD93], [CLAR95]. In comparison, only a few exist for ultrasound images due to inherent problems associated with them, such as high noise and low resolution. Fortunately, the ultrasound data used in this research is unique because they exhibit lower amounts of these characteristics. Therefore, segmentation algorithms devised for MRI and CT images are more readily applicable for evaluation on ultrasound images. Still, the presence of low noise levels, discontinuous interfaces between different tissues, and wide intensity variations within tissue types poses a tremendous challenge [SAKA95a].

Because of its lower computational and memory requirements, I chose surface rendering over volume rendering, a method that uses each pixel's color and opacity information to create 3D images [HERM90]. Using segmented data, a surface-tracking algorithm was executed to generate a surface database of polygons for a lower limb model. To design an accurately fitting prosthetic socket, the CASD system uses this surface database to recreate a 3D model of a BK amputee's residual.

1.4 Overview

The remainder of this thesis is composed of the following chapters. Chapter 2 provides details on the acquisition technique for ultrasound images identifying unique characteristics and potential difficulties. Chapter 3 presents an overview of segmentation and 3D visualization techniques with an emphasis on surface rendering methods. It also discusses the role of 3D rendering in the CASD system. Chapter 4 provides the implementation details and results of various segmentation techniques. Chapter 5 discusses 3D imaging implementation and results. Chapter 6 recaps with a conclusion and recommendations for future research.

2   The Ultrasound Image Dataset

2.1 Introduction

Ultrasound scanning technology has become very popular in medicine. The modality's increased usage can be attributed to several factors. It is non-invasive, portable, efficient, and relatively inexpensive compared to CT and MRI systems [NELS93], [SAKA95a]. Because of these attributes, ultrasound imaging was chosen by the CARD Laboratory to gather information about the surface contours and internal anatomical structures of an amputee's residual limb.

2.2 Ultrasound Image Acquisition Technique

Dr. Ping He and his research group from the Biomedical and Human Factors Engineering Department at Wright State University have developed a computer-based ultrasound scanning system specifically implemented for acquiring the images of a BK amputee's residual limb. The system used for data acquisition consists of four parts: a water tank, a patient seating device, a portable ultrasound B-scanner, and a personal computer. To prevent movement during scanning, the seat was designed to hold the thigh firmly and the tank contains a limb rest [HE94], [HE96], [XUE91].

The ultrasound images gathered by Dr. He's system are quite unique. They differ in quality and appearance from typical images gathered from other ultrasound techniques such as the example in Figure 2. Dr. He's compound image technique reduces the level of noise, thereby enhancing details within the images [HE94], [XUE91].
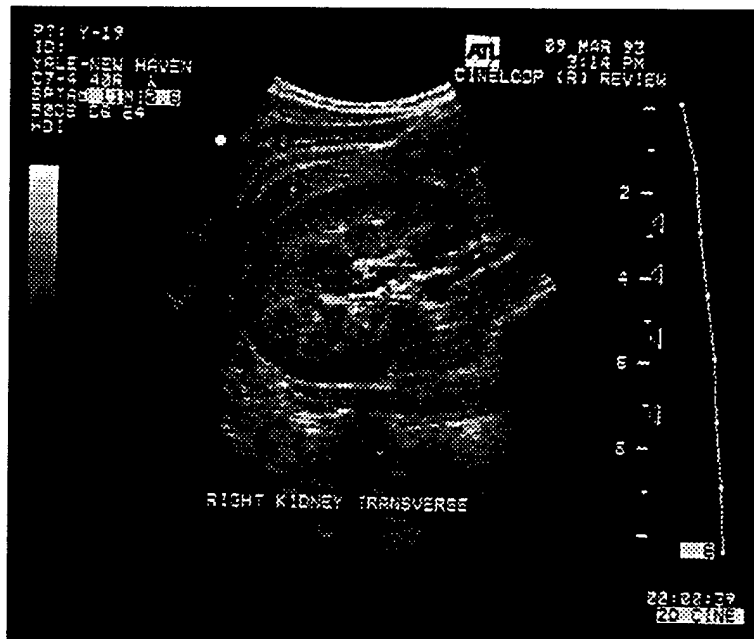
Figure 2 Typical Ultrasound Image of Kidney

Although the method's resolution depends on a number of factors, Dr. He notes that the compounding method improves the lateral resolution, which in a typical ultrasound varies with the scanning depth. Therefore, using multiple scans to reconstruct the ultrasound image of the lower limb tends to improve resolution, reduce noise, and emphasize the details of the outer skin and bone structures. See Figure 3 for a diagram of Dr. He's apparatus.
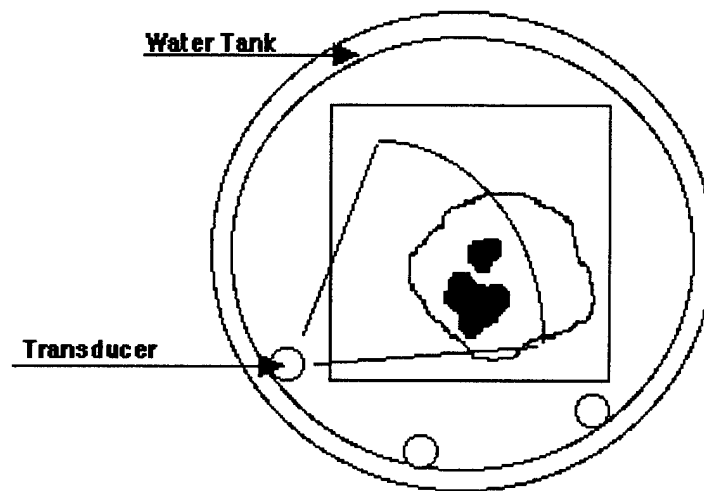
Figure 3 Diagram of Compound B-scan Method (Transducer Rotates Around Tank)

The compound imaging technique is ideally suited for this particular problem domain. The lower limb's smaller circumference allows the ultrasound transducer to easily move 360 degrees to obtain the multiple scans need to reconstruct the cross-sectional image of the residual limb. Also, the limb's simple internal structure prevents blockage of important objects of interest especially the tibia, which is the weight-bearing bone and the fibula, where the muscles attach [HE94].

Figure 4 and Figure 5 show the similarities between an accurate sketching of the internal anatomical structures and an actual cross-sectional ultrasound image obtained using Dr. He's method. The locations of the tibia and the fibula given in Figure 4 correlate very closely to the black regions bordered by bright streaks in the ultrasound image in Figure 5. The partial bright streaks surrounding the black regions show the interface boundaries between the soft tissues and bone structures.
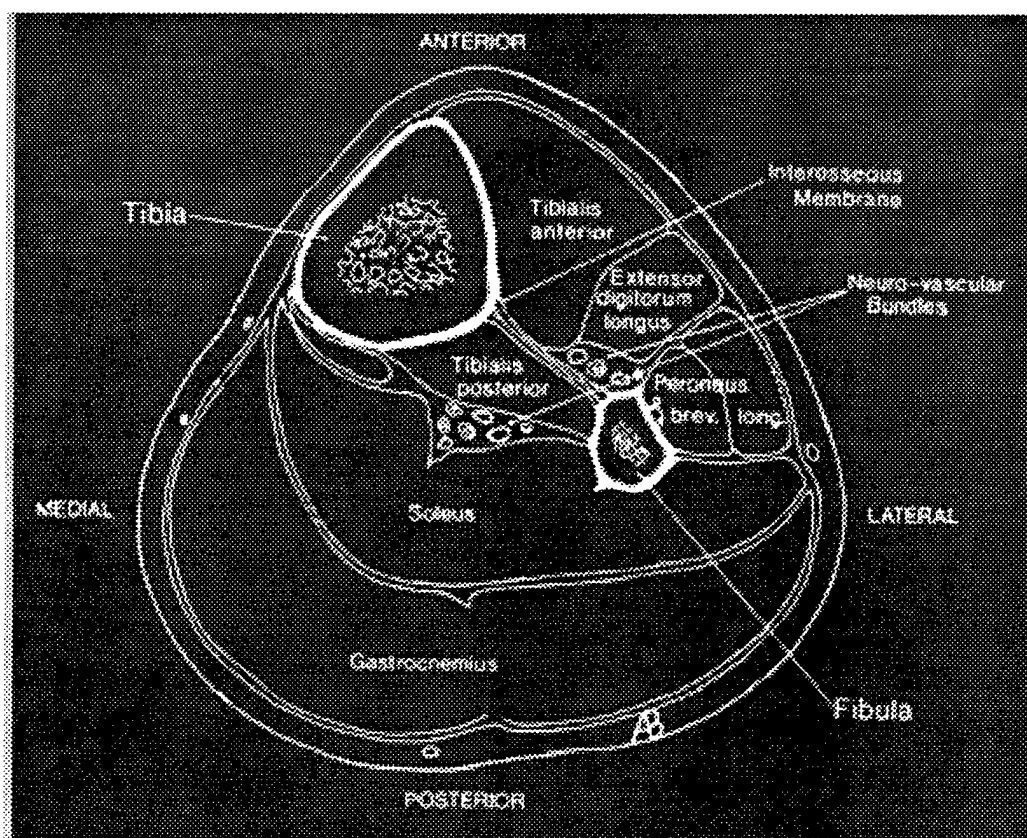
Figure 4 Anatomical Cross-section of Lower Limb [SAND86]

8
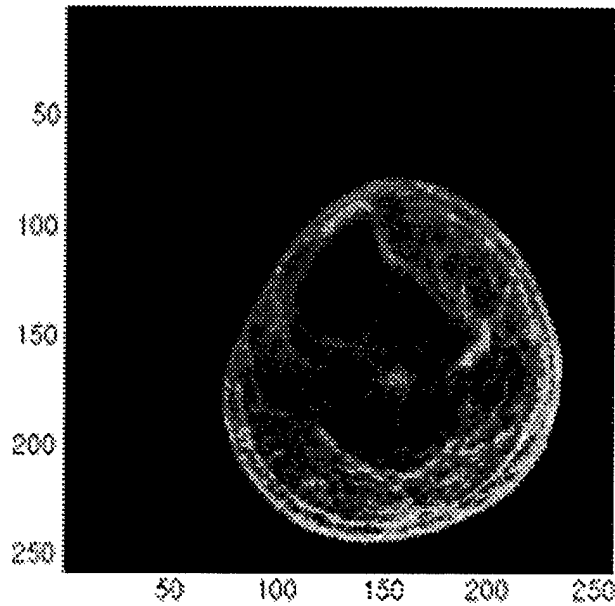
Figure 5 Ultrasound Image of Lower Limb

Each ultrasound image took approximately 12 seconds to scan and an entire dataset consisting of between 40 and 50 images of the residual limb takes between 13 and 15 minutes to produce [HE96]. The appendix at the end shows a representative set of the 20 ultrasound images used for testing the algorithms implemented in this research. Each ultrasound image measures 180 millimeters (mm) x 180 mm and has an interslice gap of 6 mm. These dimensions give an aspect ratio of 0.7 x 0.7 x 6. Each image contains 256 x 256 pixels with grayscale intensity range of 0 to 255. This dataset is a representative subset of the original dataset of 40 slices which consisted of 180 mm x 180 mm slices with 3 mm interslice gaps.

2.3 Summary

Compared to CT and MRI modalities, ultrasound imaging is inexpensive, efficient, portable and noninvasive. Because of these advantages, the CARD laboratory chose the ultrasound imaging technique to acquire cross-sectional image slices of a BK amputee's residual limb. Dr. Ping He's compound imaging technique provided the ultrasound image slices. He specially designed and developed this technique for gathering image data on BK amputee's residual limbs.

Although Dr. He's technique produces images with reduced noise and higher details, typical ultrasound problems due to noise and incomplete boundaries still exist. These problems present a challenge in processing and recreating an accurate model of the amputee's limb. To generate a lower limb model, each slice in the ultrasound image dataset needs segmentation to extract the locations of the bone structures.

3   Image Processing, Segmentation, and 3D Rendering Techniques

3.1   Introduction

Three-dimensional (3D) rendering algorithms are used to create computer-generated graphical models of human anatomical structures. These models provide precise recreations of structures from two-dimensional medical images. Visualization of 3D models help medical specialists to diagnose and analyze patients' medical problems.

The medical images are acquired through computerized tomography (CT), magnetic resonance imaging (MRI), ultrasound, and other medical modalities. Of these various modalities, ultrasound is one of three modalities capable of providing the ability to visualize both soft and bony tissue [STYT90]. This fact, along with its low cost, portability and non-invasive nature, makes ultrasound the best candidate for obtaining data about an amputee's residual limb [NELS93]. However, the special characteristics inherent in ultrasound images, such as noise and lack of complete boundaries, must also be dealt with to create accurate representations. To address these problems, ultrasound images are frequently preprocessed using image processing techniques to enhance image quality leading to more accurate segmentation.

Since my research concentrates on accurately creating a 3D lower limb model, the scope of this review will first briefly focus on image processing. Then, this review will explore segmentation, a preprocessing step for identifying objects of interest within images, and the two categories of 3D rendering -- volume rendering and surface rendering. Discussion of algorithms will be brief and will provide high-level overviews rather than including the specific steps in each algorithm.

11

3.2 Image Processing

Ultrasound images have varying amounts of noise, or speckles, that hide important details desired by physicians for 3D visualization. Image processing involves the modification of an image to produce a new image. Generally, image processing techniques are used to manipulate and enhance images so that they provide important information used in applications such as object recognition, edge detection, and image segmentation [CAST96].

Filtering, an image processing techniques, is frequently incorporated into algorithms to reduce noise levels and enhance image clarity [SAKA95a], [SAKA95b]. Filtering can be performed in one of two domains: spatial or Fourier. Spatially filtering an image by passing the filter over each image pixel is equivalent to the convolution of images in the Fourier domain [CAST96].

In their 3D rendering work, Sakas and Grimm used three different types of filters to achieve different goals. They used filters to reduce noise, smooth contours, and close gaps on fetal ultrasound images that are characterized by high levels of noise [SAKA95b]. After image enhancement, segmentation is necessary to separate different objects into appropriate tissue classes [SAKA95a], [SAKA95b], [SMIT95].

3.3 Segmentation

Due to the presence of noise and clutter in ultrasound images, automatic segmentation for identification of objects, such as the outer skin, tibia and fibula, is difficult. Gaps in the boundaries and wide variations of intensities within tissue classes further complicate the ability for unsupervised segmentation [HECK96]. For instance, without compensating for noise, conventional techniques could result in misinterpreting boundaries of random speckle spots as surfaces, and missing boundaries at contour gaps [LIN91]. At the same time, segmentation must produce accurate results in order to correctly identify contours of the bone structures within the lower limb.

In his tutorial on 3D imaging, Udupa identifies two widely used classes of segmentation algorithms: boundary-based and region-based. Boundary-based techniques provide contours of the objects of interest while region-based ones produce binary images with locations of structures given by *voxels* marked by ones and all other being zeros [UDUP91].

Voxels are the three-dimensional equivalent of pixels [STYT91]. They are small cubes identified by the x, y, and z coordinates of their centers. Figure 6 shows a diagram of a 3D dataset of ultrasound images of a limb and a voxel representation pulled out from a image slice. Each voxel's height is equal to the thickness of an image slice and each voxel has a value where meaning is based upon useful data such as intensity or density.
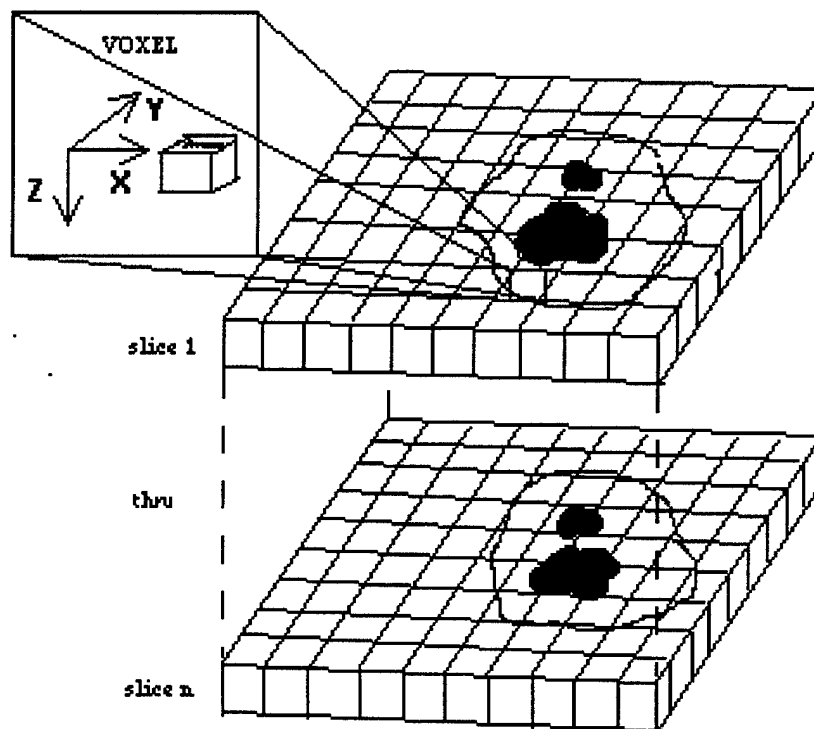
Figure 6 Voxel Representation for Dataset of Image Slices

Boundary-based segmentation, also known as edge detection, relies on the detection of rapid intensity changes within the image to find edges separating different tissues. Most boundary-based techniques rely on computing the gradient, a mathematical derivative function, that detects rapid change since edges are normally characterized by high frequencies which coincide with bright intensity streaks within ultrasound images [CLAR95], [UDUP91]. Laplacian edge detection is another technique used for boundary-based segmentation. The Laplacian, a scalar second-derivative operator, produces *zero-crossings* at edges. Castleman gives other edge operators in his book on digital image processing [CAST96].

In region-based approaches, segmentation is achieved using a set of properties that characterize voxels within the same tissue type, and distinguish them apart from others. Udupa regards thresholding to be the simplest method. It distinguishes voxels based on a specified value.

Another common region-based approach involves clustering voxels by a set of properties associated with different regions [UDUP91]. Pappas's adaptive clustering algorithm has been the basis for several research efforts in the segmentation of MRI data. His algorithm includes spatial constraints and local intensity variations. The adaptive clustering algorithm calls for moving a sliding window over an image to calculate the intensity means for that given area. Using the iterated conditional mode (ICM) approach presented by Besag in [BESA86], each pixel is inspected to maximize the conditional probability equation given as the following:

$$P(x \mid y) \quad \propto \quad \exp-[\sum_s [\frac{1}{2\sigma^2_{x_s}}(y_s - \mu_{x_s})^2] + \sum_c V_c(x)] \qquad (1)$$

where μ_{x_s} is the intensity mean for class x at pixel s, σ_{x_s} is the local noise variance, and y_s is the observed intensity mean.

Equation 1 is maximized based on the prior classification of the pixel and its local noise variance. Relying on a "pairwise interaction model" with a pixel's four neighbors, equation 1 obtains the Gibbs potential by the summation over all cliques

14

$$\sum_c V_c(x) \qquad (2)$$

where the clique potential V_C is

$$V_C(x_i, x_j) = \begin{cases} -\beta & if \quad x_i = x_j \\ +\beta & otherwise \end{cases} \qquad (3)$$

and β is the Gibbs random field (GRF) weight initially set at 1.0 with the $\Delta\beta = 0.55$. The Pappas algorithm uses the Gibbs random field to model spatial constraint during segmentation. The Gibbs potential is based on the GRF model and is the *a priori* probability of the segmentation. After a specified threshold of pixels converged, the cycle is repeated by decreasing the window size again by half until it reaches a specified minimum window size [PAPP92]. Other researchers such as Chang, Ashton, and Yan have used the Pappas clustering algorithm to develop segmentation techniques for 3D MRI scans of the brain [ASHT95b], [CHAN93], [YAN94].

Mathematical morphology, a group of image processing techniques, is also able to segment images. This approach is composed of a set of binary-operators which can be used in different combinations. Morphological operators use a structure element (SE), which acts similar to a convolution kernel, over the original image [CAST96]. The SE can be of any size and shape containing 0's and 1's and is usually designed based on knowledge of the object of interest. Thomas and Peters used several morphological operators in their research to extract femur length from fetal ultrasound images. Their method used morphological operators to reduce noise, fill in small holes in the femur, and remove unnecessary extensions from the femur [THOM91]. Other research by Sakas and Walters also tried morphological operators to reduce noise and fill in gaps on the surfaces of ultrasound images. They were investigating various types of filtering to extract surfaces from 3D ultrasound data [SAKA95a].

3.4 Methods for 3D Imaging

As mentioned previously, three-dimensional medical models created by computers result from two primary categories of 3D imaging techniques: *volume rendering* and *surface rendering* [UDUP90]. Volume rendering makes no assumptions concerning underlying structures or the surface, but instead, estimates structures using a voxel's light-reflection characteristics, and color information [UDUP90]. Surface rendering displays images with surface estimates based on image data containing information on the structures of the human body.

In general, although volume rendering tends to produce higher quality, photorealistic images, it is computationally expensive and requires more memory than surface rendering [HERM90]. Therefore, the choice in deciding between the two approaches for 3D visualization of the residual limb for the CASD system depended largely on the needs of prosthetists. Since prosthetists are not worried about the photorealism, my research investigated the use of a voxel-based surface rendering technique that not only generates images quickly but accurately. Each rendering technique is described below, but volume rendering will only be discussed briefly since this research focused on surface rendering techniques.

3.4.1 Volume Rendering Techniques

Volume rendering methods have been developed to display data directly from gray-scale volume data. Two primary techniques for volume rendering are octree encoding and ray-tracing. In octree encoding, a hierarchical data structure must be created to represent the volume data. This structure allows for direct manipulation of the 3D model, for example, slicing through images to reveal inner tissue [BARI93].

Greater efficiency, compared to the octree method, makes the ray-tracing technique more widely used for volume rendering since no preprocessing is needed to set up a hierarchical structure. Ray-tracing consists of three steps: the geometrical transformation to

align the data with the viewpoint, spatial segmentation to select only the voxels in the volume of interest, and finally gray-level segmentation to display objects of interest from the volume dataset [BARI93].

3.4.2 Surface Rendering Techniques

Newer surface rendering techniques usually rely on voxel-based methods rather than triangulation algorithms using planar contours to produce 3D representations and result in higher accuracy and reliability. Generally, these surface rendering techniques are composed of three steps: segmentation, extraction and tiling of the surface contour, and application of perspective with shading [BARI93].

Since segmentation has already been discussed, the discussion moves to the next step of surface tracking. A surface-tracking algorithm is executed to extract and tile the surface contours with polygons (usually triangles) to create a surface database. This approach starts by identifying all voxels within a dataset that have surfaces cutting through them to create a surface database [BARI93]. In the late 1980's, Lorensen and Cline presented the "marching cubes" method to detect voxels which have surfaces intersecting them and to estimate the intersecting polygons based on surface topology [LORE87].

The surfaces extracted can then be displayed using colors, shading, and illumination to create realistic 3D images. To increase realism and recognition, colors that approximate the anatomical structures are used to display the 3D model. Shading and illumination models are used to give depth and orientation cues. This final step, incorporating color, shading, and illumination, is not covered in detail here since our research is limited to achieving accurate segmentation and surface definitions of a residual limb.

3.5 CASD Systems and Role of 3D Rendering

Due to advances in technology, computer-aided socket design (CASD) and computer-aided manufacturing (CAM) research for design and fabrication of prosthetics and orthotics has

17

been rapidly progressing over the past ten years. Currently, several commercial systems are available that use CASD and/or CAM technologies [TOPP90].

One such system is the CANFIT system developed by the University of British Columbia and Shape Technologies, Inc. A clinical study compares this system with the manual form of socket fitting. The study indicated favorable results for the CANFIT system but also identified areas needing further improvement such as 3D visualization of the limb and data acquisition techniques to show internal structures as well as surface topology [TOPP90].

To acquire a model of the amputee's limb, the CANFIT system used measurements obtained by the prosthetist to match the amputee's limb to the closest fitting models in its database of nine models. The system then took these models matching a amputee's limb to extrapolate and generate a 3D representation. Because of subjectivity during measurements and a limited database, data acquisition produced inaccurate representations of the amputee's limb. As a result, this process required additional fittings to achieve acceptable results. In addition to the previously mentioned shortfalls, the system was too expensive to be used on a broad scale [TOPP90].

Another noteworthy project was at Sandia National Laboratories in New Mexico. Researchers there developed a system composed of ultrasound imaging equipment to acquire data and software composed of both commercial-off-the-shelf and customized software packages to produce 3D renderings of the limb [MORI95]. Since the Sandia system used interactive segmentation algorithms to create a 3D rendering, there is still a need to address improvements for faster, more automated segmentation.

The CASD system that Armstrong Laboratory has been creating will exhibit similarities to both of the systems mentioned above. However, a number of improvements will be incorporated into this system. Like the system at Sandia, Armstrong's system will use ultrasound imaging equipment to acquire sequences of image slices of the lower limb. The system's software will provide automated segmentation to depict the internal bone structures

and surface topology of a residual limb. Then the CASD system will be able to accurately render a 3D model of a limb for viewing and manipulation. The CARD Laboratory is also exploring automatic landmarking of pressure and relief areas on the 3D models.

3.6 Summary

Algorithms leading to 3D rendering of ultrasound datasets need to consider the special characteristics associated with them. Accurate segmentation of the ultrasound images of the residual limb is very important in providing a 3D model for the CASD system. Since numerous segmentation algorithms already exist to handle CT and MR images, the use of these algorithms on ultrasound images needs investigation. By specifically tailoring these techniques, the challenges presented by ultrasound images can be met. Using segmentation combined with surface rendering to generate a realistic 3D model of a limb provides better understanding of the surface topology and it's relationship to internal bone structures. This increases a prosthetist's ability to fabricate more comfortable prosthetic sockets in a shorter amount of time with fewer fittings.

4 Evaluation of Segmentation Techniques

4.1 Introduction

This chapter presents the implementation details and results of the four segmentation techniques evaluated in this research. Each technique's approach was reviewed for applicability to low noise ultrasound images. Since the ultrasound images used in this research contained low noise, these images may not need the extensive preprocessing of other ultrasound images. Normally, because of high noise and poor image quality, typical ultrasound scans require the use of various image processing techniques to distinguish desired detail from artifacts. The examination of each technique also ensured that algorithms did not rely on parameters dependent on a particular modality such as CT or MRI. In addition, selection was based on consideration of image types used for experimental testing. Algorithms that had been used on images similar to the ultrasound lower limb images were more favored. These selection criteria enabled overall assessment of each technique's potential for accurately segmenting the ultrasound images.

The techniques implemented in this chapter were tested using Dr. Ping He's ultrasound dataset. Figure 7 shows an ultrasound slice from his dataset. The two white outlines in the image are bounding boxes denoting locations of the bone structures in the lower limb. These bone regions were manually identified based on anatomical knowledge and known ultrasound characteristics of bone structures. To aid in comparison, most figures in the result sections display composite images. A composite image has the original ultrasound image overlaid with the boundary outlines from the segmented image.

20
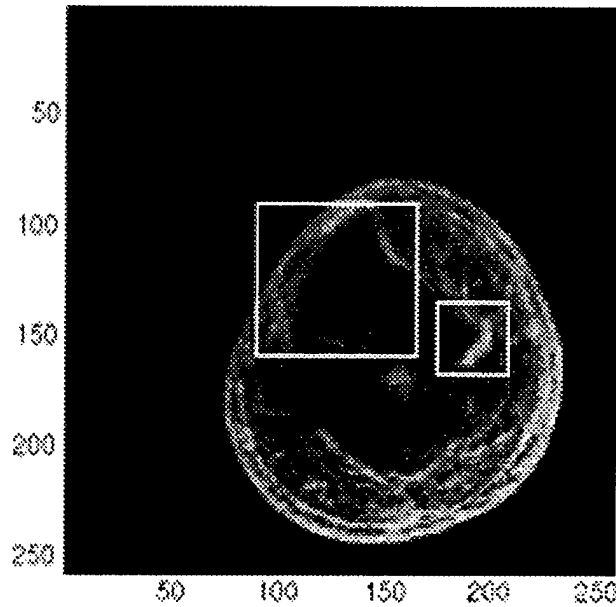
Figure 7 Locations of Bone Structures in Original Image

4.2 Multiresolution Bayesian Segmentation

Examination of previous research efforts in the use of a Bayesian approach provided evidence for its potential success in segmentation of noisy images. In an earlier research effort, the Bayesian technique accurately detected and analyzed surface classifications and normals on noisy ultrasound images [LIN91]. In two other efforts, the Bayesian approach provided accurate, automated segmentation of MRI brain scans [CHAN93], [YAN94]. According to Sakas and Walter, a multiresolution framework allows for elimination of noise and minor structures faster than important surfaces. This happens because smaller artifacts have lower coherency while larger surfaces are still detectable at lower resolutions [SAKA95a].

Supported by these previous efforts, the multiresolution Bayesian approach presented by Ashton and Parker was selected for its ability to reduce speckles and accurately segment noisy 2D ultrasound images. The developers of this algorithm tested their approach on

21

transesophageal echocardiographic scans of the human heart. The specialized algorithm takes

into account the statistical nature of ultrasound data to process and segment images [ASHT94a],

[ASHT95a]. The following paragraphs summarize the implementation of this algorithm.

4.2.1 *Approach and Implementation Of Original Algorithm*

This Bayesian algorithm initially applies a low-pass filter to remove speckles from the

original ultrasound images. The filter, constructed to characterize and reduce the speckles, has

to optimally maximize two goals: noise elimination and preservation of important edge detail.

The filter suggested by Ashton and Parker is a finite impulse response (FIR) filter. The FIR

filter is implemented as a Gaussian with a response equal to twice the diameter of the estimated

speckle spot size n.

To increase speed, the FIR filter is implemented in the Fourier domain. First, an image

of the filter is constructed using a multivariate Gaussian distribution. The original image and

the filter image have to be the same image size with dimensions based on powers of two.

Then, both images are fast Fourier transformed and convolved. The convolved image are then

inverse Fourier transformed back to the spatial domain to produce a filtered version of the

original image.

The speckle spot size n is an important filter parameter. Varying the size of the speckle

spot parameter affects the resulting image. The larger the speckle spot size (or diameter of the

Gaussian), the lower the frequencies passed. In other words, a smoother image results.

Increasing the smoothing factor of the filtered image can cause the loss of important boundary or

edge definition. Therefore, the speckle spot size has to be carefully chosen.

After filtering, the image is segmented with a K-means clustering algorithm to calculate

each pixel's initial intensity-based classification. The K-means algorithm finds the k number of

intensity means that an image's intensity values cluster around. These k intensity means are

22

used to classify each pixel in the image. This initial classification provides the basis for the adaptive clustering algorithm.

Ashton and Parker created a modified version of the Pappas adaptive clustering algorithm summarized in Chapter 3 to use as the backbone of their algorithm. Their modified adaptive clustering algorithm classifies each pixel based on local averaging using the intensity means of surrounding pixels. The classification of the pixel's four neighbors, which form four-pairwise cliques with the pixel, is also considered as well as its local noise variance when maximizing the conditional probability function given in Equation 4.

The adaptive clustering algorithm is initially executed on the lowest resolution image resulting from the decimation of the filtered image by the original speckle spot size n. After maximization of Equation 4, this process continues to the next higher resolution by replicating to the original image size followed by decimation where $n = n - 1$. Upon reaching the highest resolution, equivalent to the original image size, a final execution of the adaptive clustering algorithm produces the final pixel classifications for the segmented image.

Equation 1 given in Chapter 3 is modified to maximize the conditional probability equation given as the following:

$$P(x \mid y) \quad \propto \quad \prod_s (\frac{1}{\sigma_{x_s}})\exp-[\sum_s [\frac{1}{2\sigma_{x_s}^2}(y_s - \mu_{x_s})^2] + \sum_c V_c(x)] \qquad (4)$$

where μ_{x_s} is the intensity mean for class x at pixel s, σ_{x_s} is the local noise variance, and y_s is the observed intensity mean. This modification by Ashton and Parker accounts for the fact that ultrasound images are not corrupted by globally-uniform Gaussian noise. However, since Gaussian statistics are easier to represent mathematically than Rayleigh statistics, they assumed a Gaussian distribution for pixels within a given region where σ_{x_s}, the local noise variance, is estimated independently for each class and is proportional to the local class mean. After a

specified number of pixels converged, the local noise variance is recalculated and the cycle is repeated by decreasing the window size again by half until it reaches a specified minimum window size. The general steps of the algorithm are as follows:

1. Low-pass filter the original image with a Gaussian filter of diameter 2n x 2n. Decimate image by n (the size of speckles).
2. Obtain initial cluster estimates by K-means.
3. Set the GRF weight to an initial value.
4. Apply the clustering algorithm.
5. Expand the cluster matrix by n and then decimate by n-1.
6. Decrease n by 1.
7. Lowpass filter and decimate the original image by new n.
8. If n > 1 then increase GRF weight and go to step 4.
9. Apply clustering algorithm a final time on original image.

4.2.2 Results of Original Algorithm

The original 2D multiresolution Bayesian approach produced a segmented image that contained artifacts within the limb and did not correctly distinguish bone structures from the artifacts. Because of noise and wide intensity variations throughout the images, segmentation identified numerous regions within the limb as bone structures. Therefore, this segmentation does not accurately identify bone locations which are vital for generating 3D surface models of outer skin and two bone contours in a lower limb. Figure 8 shows a composite of an original image with contours of a segmented image.
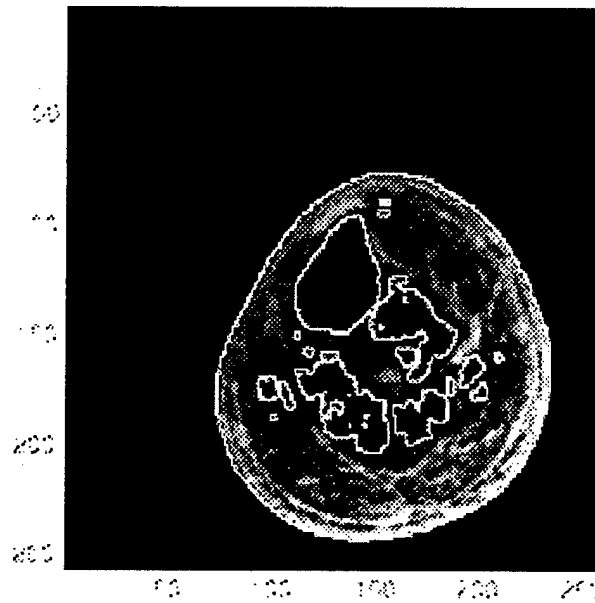
Figure 8 Segmented Image Using Original 2D Bayesian

4.2.3 *Approach and Implementation of Enhanced Algorithm*

Morphological operators based on shape characteristics are frequently used in image processing. As described in Chapter 3, a structure element (SE) acts similar to a convolution kernel and is passed over each pixel in the original image. The morphological operation of *dilation* fills in holes in the image that are equal to or smaller than the size of the structure element. The morphological operation of *erosion* removes small clusters that are smaller than a given structure element. When erosion follows dilation of images, this is known as a *closing* operation [LYBA94]. Combined in this manner, these operators can help remove noise or artifacts, and refine contours producing better segmentation than algorithms that lack morphological operators [SAKA95a], [THOM91]. Due to these benefits, this research developed new enhancements for use in conjunction with the 2D Bayesian technique. Morphological operators were combined with the 2D Bayesian to extract of bone regions from artifacts.

To enhance Bayesian segmentation of the ultrasound image, a binary image of each image's potential bone regions is created by applying a mask to the segmented image. Then

25

execution of the closing morphological operator removes small artifacts and refines contours of candidate bone regions. The remaining image of potential bone regions requires further processing with additional discriminators to distinguish the tibia and fibula from artifacts. These discriminators remove regions not meeting certain size, shape, and location criteria associated with the two bone (tibia and fibula) regions.

To extract the two bone structures, the enhanced Bayesian algorithm uniquely labels each region of contiguous pixels by looking at their 8-connected neighbors. Using the labels, this algorithm then calculates each region's size and identifies the largest region as the tibia. After the selection of the tibia, the algorithm searches for potential fibula candidates by checking the remaining candidates' sizes to see if they are at least 1/6 the size of the tibia. This ratio was chosen after evaluating several values.

For further evaluation of potential fibula candidates, the algorithm compares each candidate's distance from the tibia for closeness and shape for circularity. It calculates the distance from the center points of the bounding boxes for the tibia and fibula regions and weights this by 0.7. Circularity is assigned a weight of 0.3. These weights were determined by observation of the ultrasound dataset and may need adjustments with further testing of more ultrasound datasets. Examining initially segmented images, the minimum distance of the fibula region to the tibia is more important than the region's overall roundness. The final candidate having the minimum weighted distance and shape is identified as the fibula.

Following identification of bone structures, the enhanced implementation assigns pixels of each tissue class a specific intensity of 50 for the limb and 255 for each of the two bones. These values are used later in chapter 5 as the isovalues for the "marching cubes" algorithm.

For fast prototyping and quick results, the enhanced multiresolution Bayesian approach was implemented using MATLAB version 4.2 on the SGI workstations. MATLAB code was written to input segmented images and perform the extraction of bone regions. The code used built-in morphological operators to perform the closing operation with a structure element 10

voxels in diameter. All enhancements except for the closing operation were incorporated into the original Bayesian segmentation algorithm in C++.

4.2.4 Results of Enhanced Algorithm

The modified, enhanced version evaluated and distinguished the tibia quite accurately . The results were verified by Dr. Ping He and Dr. Kefu Xue, two biomedical experts in ultrasound imaging from Wright State University. They also observed that segmentation of the tibia appeared quite accurate. The tibia's accuracy is important for an amputee's residual limb since this bone is load-bearing.

Without the closing morphological operator, the tibia's back shadow in the ultrasound image detracted from segmentation of the fibula and led to elongated and misshapen contours. Figure 9 displays a segmented image without a closing operator. Inclusion of the closing morphological operator in the enhanced Bayesian algorithm helped to refine the contours of the bones. In comparison to Figure 9, the composite image in Figure 10 shows more accurately defined bone contours resulting from the closing operator. Appendix B and Appendix C show the entire segmented dataset of ultrasound images using the original and enhanced algorithms.
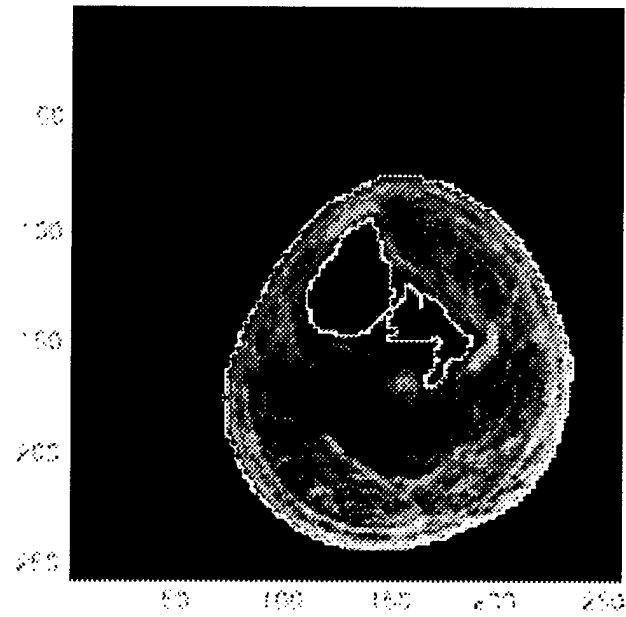
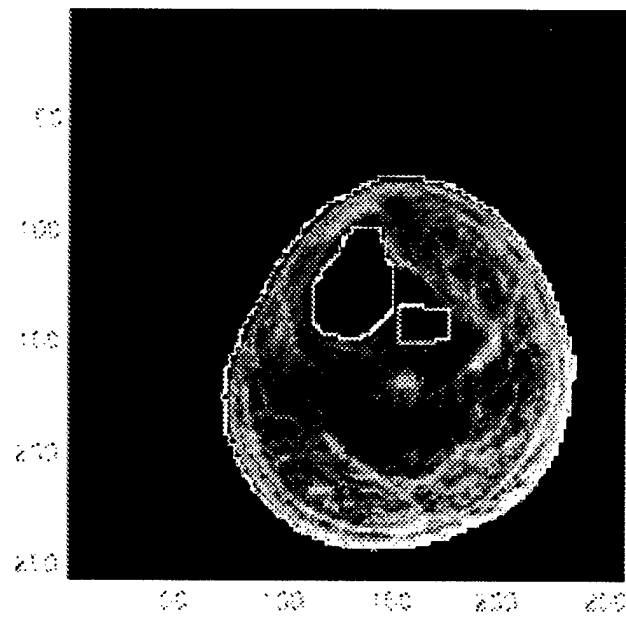*Figure 9 Enhanced Segmented Image Without Closing*

Figure 10 Enhanced Segmented Image With Closing

4.3 Three Dimensional Bayesian Segmentation

Three dimensional (3D) segmentation takes into account the relationship of a pixel to its adjacent slice neighbors as well as its intraslice neighbors. As a result, 3D segmentation allows connectivity and smoothness constraints to be imposed in 3D and may increase accuracy [CHAN93]. Therefore, by modifying the original algorithm described in section 4.2 for multiresolution Bayesian to include 3D segmentation, the ultrasound dataset may be more accurately segmented.

4.3.1 Approach and Implementation

The 3D Bayesian technique is similar to the previously described 2D version. The 3D Bayesian technique relies on the modified adaptive clustering algorithm and Besag's ICM to maximize a pixel's conditional probability based on its relationship with all neighboring pixels between and within slices [ASHT94b], [ASHT95b], [CHAN93], [YAN94]. Unlike the previous technique, the 3D Bayesian approach does not apply filtering before segmenting each image. However, to take into account the Gibbs potential between neighboring interslice pixels, the clique potential is extended to 3D as follows:

$$V_{uv}(x_i, x_j) = \begin{cases} -\beta_1 & \text{if } x_i = x_j \\ +\beta_1 & \text{otherwise} \end{cases} \tag{5}$$

$$V_{w}(x_i, x_k) = \begin{cases} -\beta_2 & \text{if } x_i = x_k \\ +\beta_2 & \text{otherwise} \end{cases} \tag{6}$$

with the Gibbs potential given by the sum of all clique potentials between the four intraslice neighbors and two adjacent slice neighbors. The intraslice Gibbs weight is set at $\beta_1 = 2.0$ and the adjacent slice Gibbs weight at $\beta_2 = 0.12$. These weights are calculated based on an intraslice resolution of 0.7 mm and an adjacent slice resolution of 6.0 mm using the ratios given in [CHAN93]. Therefore, the pixels are more likely to be in the same class as their intraslice neighbors than their interslice ones.

Like the 2D version, the 3D approach initially classifies the pixels in each slice by applying K-means clustering. Then for each slice of the 3D dataset, the adaptive clustering algorithm is maximized after substituting the extended clique potentials given by Equation 4 and Equation 5 into the conditional probability formula from Equation 1 [CHAN93].

4.3.2 Results of 3D Bayesian

Applying the 3D Bayesian approach did not yield better results than the 2D method because of the low interslice resolution between slices and the presence of noise in the ultrasound images. The image in Figure 11 shows the segmented image produced by the algorithm and shows the increased presence of artifacts due to noise.

Preprocessing all ultrasound slices in the dataset with a FIR filter (a Gaussian with diameter of 2n x 2n where the speckle spot size is n = 2) produced segmented images that closely resembled images from the original 2D Bayesian. The filter reduced the level of noise in the ultrasound slices and reduced the artifacts present in the segmented data. Figure 12 shows a filtered image from the 3D dataset that looks similar to the image slice 1 given in Appendix B.
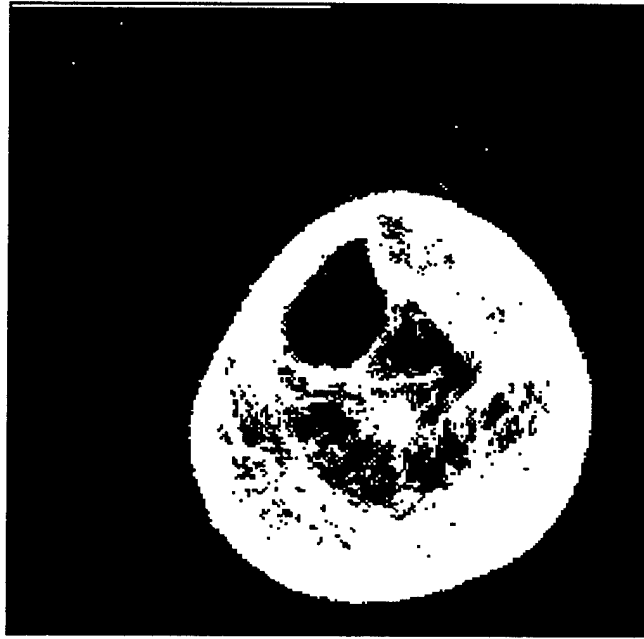
Figure 11 3D Bayesian Segmented Image

Figure 12 Segmented Image Using 3D Bayesian with Filtering

4.4 Marr-Hildreth and Morphological Operators

Edge detection algorithms can be applied during segmentation of MR images. Bomans' work, which combines edge detection and morphological operators, was chosen to explore the effectiveness of boundary-based techniques on ultrasound images. Bomans used a 3D Marr-Hildreth operator along with the dilation and erosion morphological operators to segment magnetic resonance images of a human head for 3D rendering. As mentioned during the discussion of the enhanced Bayesian technique, the use of morphological operators tends to refine contours while removing artifacts. Bomans' technique resulted in accurate segmentation of MRI brain [BOMA90].

4.4.1 Approach and Implementation

Using *zero crossings*, the locations of intensity changes, the Marr-Hildreth edge operator can detect anatomical structures contained in images. The Marr-Hildreth operator is defined by the following:

$$E(x,y,z) = \nabla^2(I(x,y,z) * G(x,y,z,\sigma)) \tag{7}$$

where ∇^2 is the Laplacian operator, $I(x,y,z)$ is the image, $G(x,y,z,\sigma)$ is the Gaussian, and $E(x,y,z)$ is the image of edges. The operator smoothes the data to remove areas of high frequency and uses a Laplacian to detect edges regardless of orientation [CAST96]. Then 3D morphological operators of dilation and erosion are applied to enhance surface contour definition. With these surface contours, Bomans generated a realistic 3D display of the head consisting of skin, bone, brain, and the ventricles [BOMA90]. This implementation does not go into the other steps used by Bomans, et al. to obtain the 3D rendering since the area of focus was the comparison of segmentation approaches on this type of ultrasound images.

MATLAB was used to generate the code and test this approach on the ultrasound images of the lower limb. Slight modification of MATLAB's built-in functions of the 2D Marr-

Hildreth edge operator and the 2D closing morphological allowed for the testing of their effectiveness in segmenting the ultrasound images. The Marr-Hildreth operator was modified to approximate a Laplacian of a Gaussian using the Difference of Gaussians as given below [BOMA90]. Also, the MATLAB's closing operator's structure element was modified to a disk shape of diameter 5. Although Bomans extended these operators to three dimensions, the two dimensional operators in MATLAB were able to provide a general idea of how this approach would segment ultrasound images. If the 2D methods in MATLAB provided better segmentation of the skin and bone regions than the previous techniques, then implementation in 3D may yield similar or better results.

This implementation is similar to Bomans approach of using a difference of Gaussian (DOG) operator to estimate the Laplacian of a Gaussian or $\nabla^2 G$ operator defined as

$$\nabla^2 G(x,y,z,\sigma) = G(x,y,z,\sigma_e) - G(x,y,z,\sigma_i) \tag{8}$$

Bomans used the DOG operator to reduce memory requirements and lower the number of convolutions. If a DOG operator is used to approximate the $\nabla^2 G$ operator then the standard deviations σ_e and σ_i are set to make the filter bandwidth small and the sensitivity large. The ratio of $\sigma_i : \sigma_e$ was 1.6 where

$$\sigma_e = \sigma \cdot \sqrt{\frac{1-(1/r^2)}{2 \ln r}} \tag{9}$$

$$\sigma_i = r \cdot \sigma_e \tag{10}$$

and $r = 1.6$ and $\sigma_e = 0.805 \cdot \sigma$ and $\sigma_i = 1.288 \cdot \sigma$ [BOMA90]. This implementation attempted standard deviations of $\sigma = 1.0, 2.0,$ and 3.0 to examine the difference in the resulting images. The best results came from using standard deviation of 1.0. For the morphological operators, dilation and erosion, a structuring element of both 5-voxel diameter and 10-voxel

diameter was applied to close the binary images from the Marr-Hildreth operator to eliminate small holes and smooth out contours.

4.4.2 Results of Marr-Hildreth and Morphological Operators

Using the algorithm developed by Bomans with a structure element (SE) of diameter 5 did not produce good results. The structure element was not big enough to eliminate small artifacts after the edge operation. As a result, the final image had artifacts and the technique did not detect the bone structures as well as the enhanced 2D Bayesian approach. Figure 13 shows two images: the top shows all edges detected using the Marr-Hildreth operator and the bottom shows the new image after the closing operation. Since the morphological operators rely on size and shape characteristics, the SE diameter was increased to 10 to remove the small circular artifacts shown by the lower image in Figure 13. This size eliminated most of the artifacts and left two regions remaining that correspond closer to the locations of the bone structures. The final segmented image was similar to the one obtained from the enhanced 2D Bayesian technique. However, this approach introduced two small protruding artifacts along the upper skin contour of the limb due to the presence of noise clusters. Figure 14 shows the result of reapplying the edge operator and the closing operator with SE of 10. The enhanced 2D Bayesian technique provides better segmentation without introducing additional artifacts in the final segmented image.
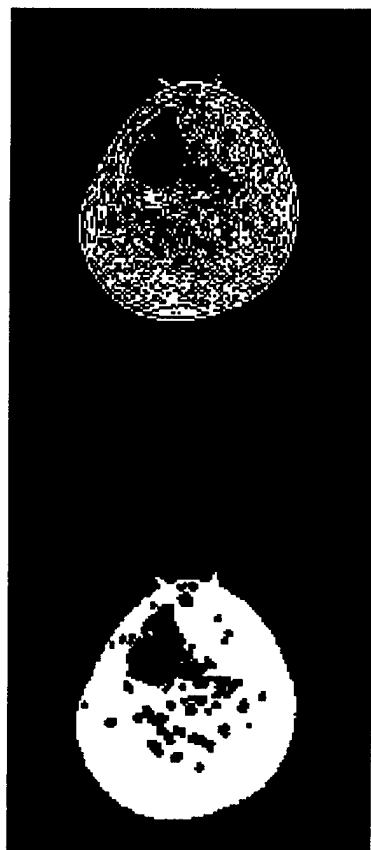
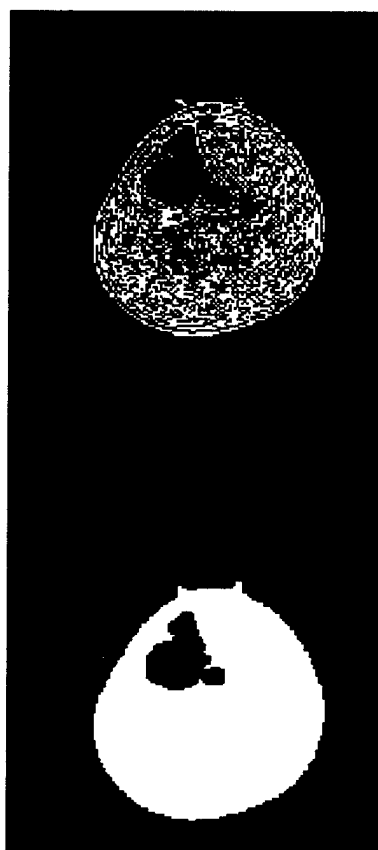Figure 13 Marr-Hildreth and Closing with SE 5

Figure 14 Marr-Hildreth and Closing with SE 10

4.5 Contour Searching with Genetic Algorithm (GA)

Heckman and Krumm of Sandia National Laboratories developed a boundary-based segmentation algorithm designed for ultrasound images of the lower limb (similar to Dr. He's images). According to their research, automatic segmentation of these images is difficult because of various amounts of noise and "complicated interactions between ultrasonic pulses and human tissue" [HECK96].

Edge finding and region growing techniques do not work well and without postprocessing tend to produce artifacts caused by noise and incomplete boundaries. Heckman and Krumm also state that *snakes*, a contouring method based on spatial derivatives, did not work well with ultrasound images and required an accurate starting position. The presence of noise diverted the snakes' contours from the actual boundaries in the images [HECK96].

To overcome these difficulties, the authors used a genetic algorithm (GA). The GA searches for the best-fitting, closed contours given by a closed cubic spline to the original image of the outer skin and bone structures. Their approach is similar to the Hough transform, a powerful image processing technique used to detect edges, because it globally searches for the correct contours. However, their technique is also able to conform to the complex shapes present in the images [HECK96].

4.5.1 Approach and Implementation

The GA tries to optimize a fitness function in its search for the best fitting contour in a very large search space. The algorithm represents the fitness variables with a string of symbols. Then, the GA randomly creates a *population*, a set of the strings, to begin the search and the fitness function is calculated for each member of the population. Mutation, crossover, and selection techniques are also applied to each member until one member obtains the appropriate fitness level. Specifically, mutation produces the global optimum; crossover creates

high fitness members using parts of other high fitness strings; and selection tries to choose high fitness strings by using a biased probability distribution to pick them randomly [HECK96].

The closed cubic splines used to model contours have four control points which allow for fairly smooth contours while reducing the search space. Since the search space is still quite large, Heck and Krumm's algorithm aligns initial control points to likely boundaries or high intensity regions in the image to speed up the search process. Before correlating the contours to the original image, each contour is refined to fall on "peaks of nearby intensity ridges" of the original data to compensate for discontinuities. This refinement process places perpendicular search lines along the contours to locate maximum intensity values that are used to align contours. After refinement, contours are modified with a point spread function to simulate how they would look in a real ultrasound image [HECK96]. To decrease the search space and make the computing less intensive, the authors designed the GA to search each contour separately. In addition, the GA requires a known bounding box for each contour's location so that the algorithm does not incorrectly chose large areas of low intensity with high fitness as the best contours [HECK96].

The C source code for this algorithm was obtained from the authors and compiled on a SGI workstation. The control file, which includes such parameters as the point spread function, bounding box, and data filename, was modified to test the algorithm over the ultrasound images.

4.5.2 Results of Genetic Algorithm

The genetic algorithm technique presented by Heckman and Krumm was tested on several ultrasound images. The control file for each image was modified to use the correct bounding boxes for the location of the bone structures. It took approximately 20 minutes on a SGI Indigo 2 to find the three best-fitting contours for the outer skin, tibia, and fibula.
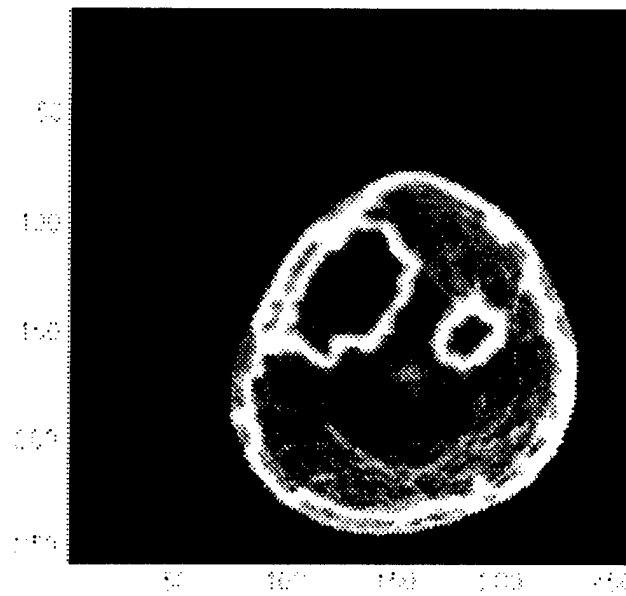
Figure 15 Contours from GA

The composite image of the resulting contours and original image shown in Figure 15 does not exhibit smooth boundary contours. The presence of noise within the image and the wide intensity variations were the factors that caused the irregular contours. To compensate, the search lines used to align the contours of the closed cubic spline to an image's intensity peaks were shortened. With this modification, the GA generated smoother contours that were less sensitive to noise and clutter in the images. Figure 16 shows a new GA composite image with smoother contours.
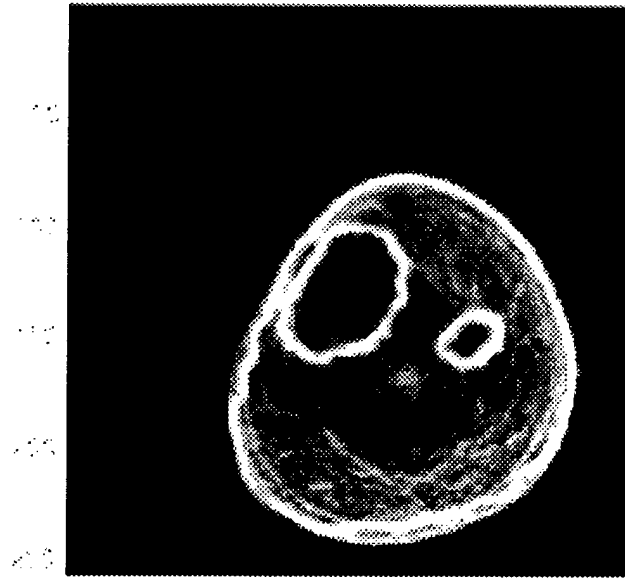
Figure 16 Smoother Contours with Modified GA Parameter

The bounding box parameters for each slice were manually located and placed in a control file since each image slice varies slightly. This step was later automated by executing the enhanced 2D Bayesian technique on each image slice to extract bone regions. Then the bounding boxes associated with the outer skin and each bone region were written to a control file for use by the GA to find the best-fitting contours.

4.6 Summary

Unless otherwise noted, all source code was implemented with the C++ object-oriented programming language and compiled using the CC Silicon Graphics (SGI) compiler. All code was compiled and tested on a SGI Indigo 2 workstation equipped with a 250 MHz microprocessor and 192 MB of RAM running the IRIS 6.2 operating system.

All segmentation techniques were evaluated using 8 to 10 ultrasound images from the dataset of 20 images. This subset of images was adequate due to lack of complex bone

structures and similar anatomical characteristics between ultrasound slices of a BK amputee's residual limb. Figure 17 gives timing results for the segmentation algorithms presented in this chapter.

Segmentation Technique	Average Time to Process an Ultrasound Slice
Original 2D Bayesian	2.9 seconds
Enhanced 2D Bayesian	15.6 seconds
3D Bayesian	28.9 seconds
Marr-Hildreth and Morphological Operators	8.6 seconds
Genetic Algorithm	18.2 minutes

Figure 17 Timing Results for Segmentation

The four major segmentation techniques implemented in this research were chosen based on their appropriateness and potential for accurately segmenting ultrasound images of the lower limb. Both the 2D multiresolution and 3D Bayesian techniques rely on a region-based segmentation approach. Both techniques use an adaptive clustering algorithm that takes into account spatial constraints and local intensity changes. The 2D Bayesian approach required further enhancement to accurately distinguish bone region in the ultrasound images. Like the 2D Bayesian, the filtered 3D approach produced similar segmented images that required more postprocessing. The last two techniques are boundary-based segmentation approaches. One combined an edge detection operator with morphological operators. The other used a model-driven genetic algorithm that searches for the best-fitting contours using a fitness function. Out of the four techniques, the enhanced 2D Bayesian produced the best overall segmentation in terms of accurately extracting bone structures and processing speed. The two techniques with faster processing times did not accurately segment the bone regions in the ultrasound images.

5 Generation of Surface Polygonal Database

5.1 Introduction

This chapter presents a method using public-domain software to create a 3D lower limb model that can be used by a CASD system to obtain underlying bone structures. Since the enhanced 2D Bayesian provides the best overall segmentation in terms of accuracy and processing time, this was the only technique used to segment and create a realistic lower limb model. After segmentation to identify boundaries of different tissues (the skin and two bones), the Visualization Toolkit version 1.1 was used to produce the surface database of polygons (triangles) and render the lower limb model.

The Visualization Toolkit (VTK) is an object-oriented C++ library of data objects and algorithms for 3D rendering written by William Schroeder, Bill Lorenson and Ken Martin [SCHR96]. The authors designed the library specifically for scientific and medical visualization. Their goal was to develop the library for easy use by novices and experts alike. VTK is public domain software available on the World Wide Web or a CD that comes with the book written by the authors.

VTK uses a pipeline architecture to process and manipulate the data for rendering [SCHR96]. Figure 18 illustrates the data flow of the architecture. A data source provides the input for visualization that is stored as a VTK data object. The VTK object can then be processed with one or more filters such as "marching cubes", decimation, or contouring filters. The data output from the filter is also stored as a VTK data object. The data can be mapped to geometric primitives for graphical display using OpenGL or GL on the SGI workstations or written out to a file.
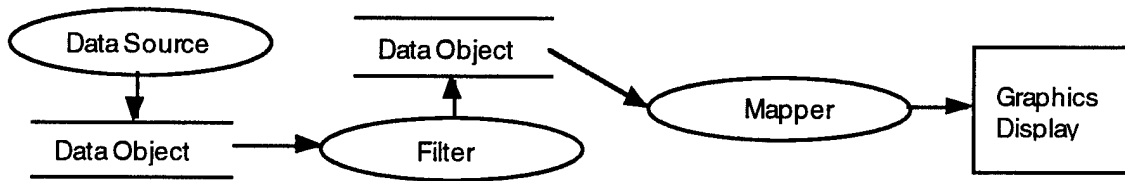
Figure 18 Data Flow Through VTK Pipeline Architecture

5.2 3D Surface Rendering Using VTK

For this research, VTK's "marching cubes" filter was chosen to create a lower limb model from the ultrasound images. The "marching cubes" filter identifies the polygons cutting through each voxel for given isovalues of each tissue class and creates a skin contour of the original image dataset. However, accurate extraction of bone structures requires use of segmented image data. The segmented image slices are better for creating the surface contours since there are continuous boundary definitions and constant intensity values associated with the outer skin and bone structures.

Before VTK could be used to *decimate*, or reduce the number of polygons defining contours, the data for the skin and bone contours has to be processed using a cleaning filter to eliminate redundant polygons generated by the "marching cubes" filter. Then to eliminate noise and artifacts, a connectivity filter extracts the largest connected contour belonging to the outer skin of the limb. Afterwards, the data is piped to a VTK filter for checking polygon normals. This process ensures that each polygon's normal correctly identifies the front and back faces of the skin and bone surfaces. Finally, the surface model of the limb is colored and illuminated with VTK's built-in OpenGL methods to create a realistic 3D rendering that can be rotated and zoomed in and out for better viewing. Each set of polygons for the outer skin and bones is also written to a file in a MOVIE.BYU formate to be imported by CARD Laboratory's system. Figure 19 diagrams each of the VTK classes created to generate graphics and output data to MOVIE.BYU file format of the lower limb model.
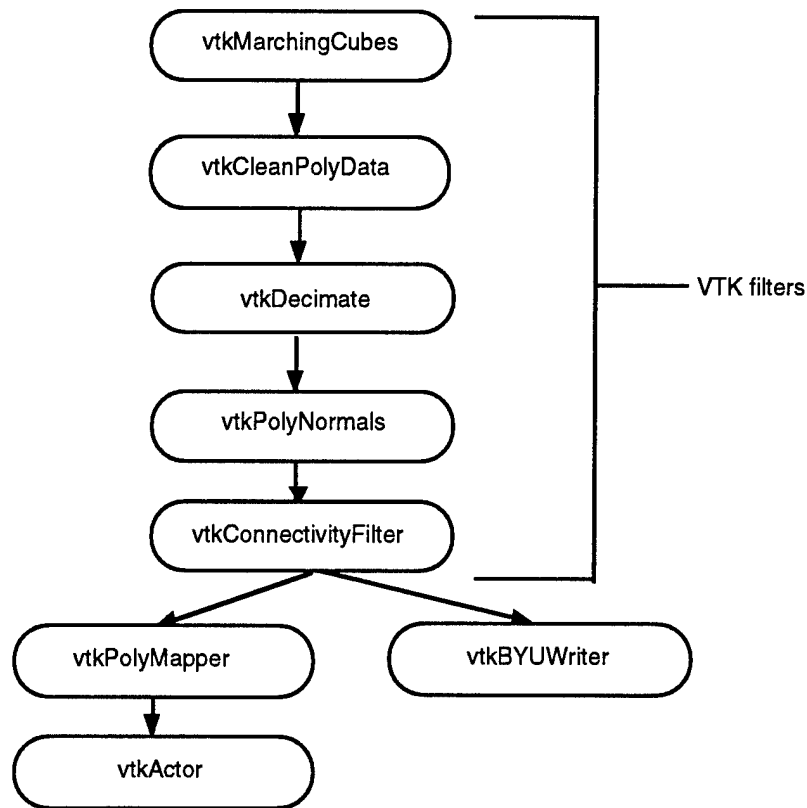
42

Figure 19 VTK Classes Called to Model Lower Limb

An additional VTK class was written to read in the raw binary image files and store the data as a VTK data structure. A special VTK class was also written to output the results of the connectivity filter to the MOVIE.BYU format. The executable relies on the use of a configuration file that has the directory path of the data files, image slice range, isovalue, and aspect ratios for the x, y, and z dimensions.

5.3 Results of Using VTK

Usually, a 3D model can be generated using the "marching cubes" algorithm on the original ultrasound dataset. However, due to noise and widely varying intensities throughout the image (even within similar tissue classes), the "marching cubes" technique without any preprocessing did not result in an accurate 3D model. Figure 20 shows the 3D representation obscured by noise and artifacts.

The model produced by merely using the segmented image slices for input into the VTK procedure did not produce smooth contours for the outer skin. Due to step-like intensity changes at the boundaries, the skin surface contour had a very jagged appearance. Figure 21 displays the lower limb model from segmented images.
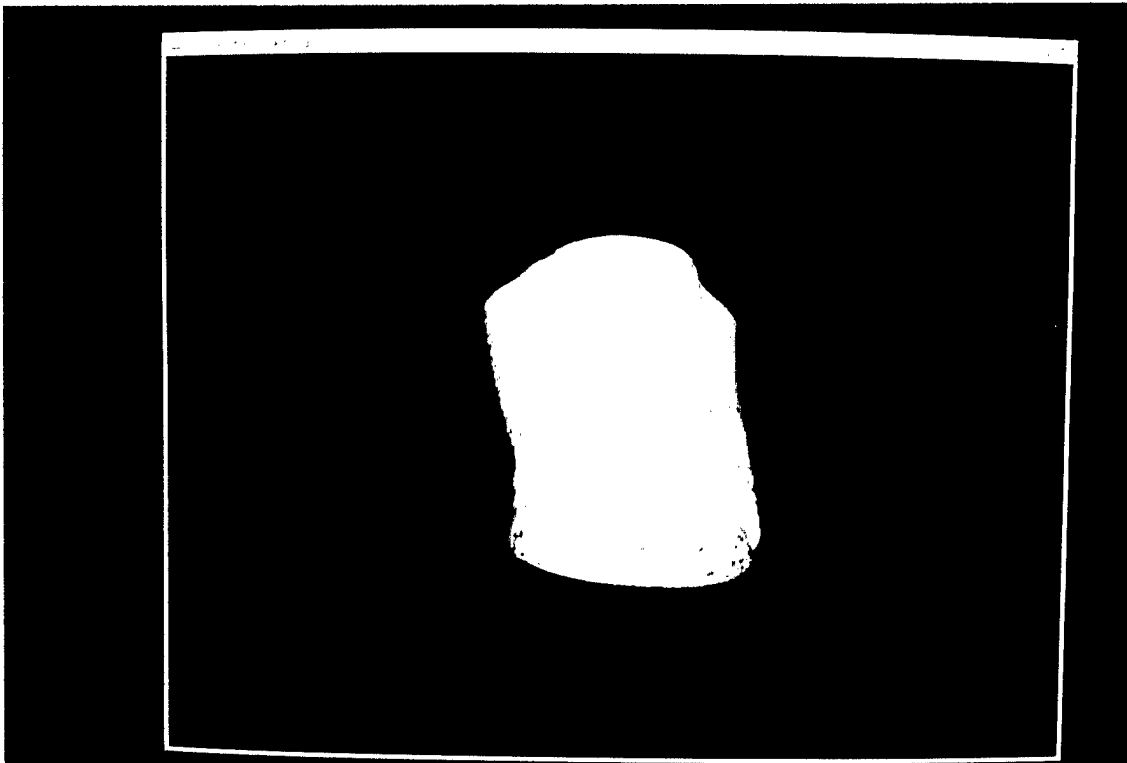

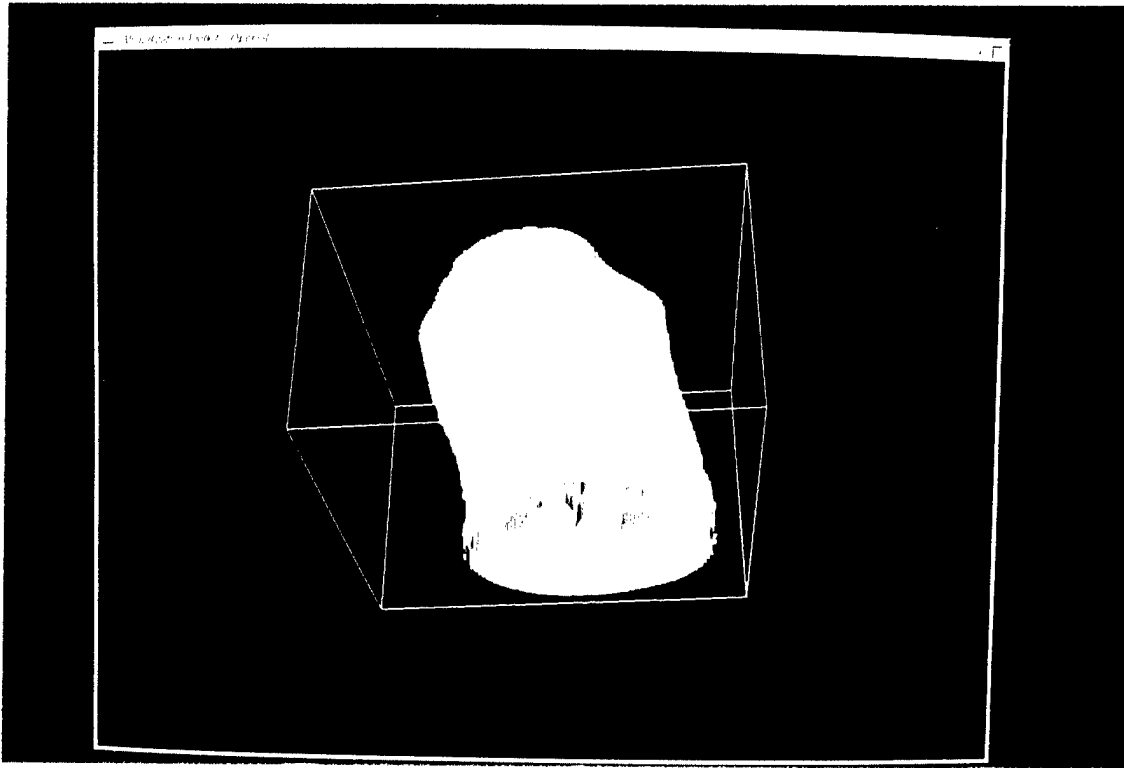
Figure 20 3D Model Created Using Only Marching Cubes

Figure 21 3D Model of Lower Limb from Segmented Images

To address these problems, a subsampled set of images was created using MATLAB's *imresize*, a function that reduces and filters an image, on the original ultrasound dataset. This new set of images was substituted for the segmented images. Applying all the VTK classes shown in Figure 19 on the subsampled images created polygons defining the outer skin contour. The subsampled 64 x 64 pixel images with aspect ratio of 2.8 x 2.8 x 6 produced more realistic, smoother skin contours.

Since the bones structures could not easily be detected using the original dataset, the segmented 256 x 256 pixel images were used to more accurately reconstruct the bone structures with aspect ratio of 0.7 x 0.7 x 6. Although this produced a smooth outer skin contour and accurately portrayed underlying bone structures (Figure 22 shows a new lower limb model), there were several tiny holes present in the model. These holes resulted from the lack of

constant intensity values for the boundary definitions in the images. Since the ultrasound images originally had wide intensity variations with bright streaks marking the boundaries, the gaps in the boundaries produced the holes present in the model. These holes did not result with use of segmented images since they have specific intensity values associated with different tissue regions. Therefore, VTK's "marching cubes" filter a connected set of polygons that completely define the skin contour.

5.4 Summary

The VTK library created by Schroeder, Lorensen and Martin provides a fast object-oriented architecture for visualizing 3D medical images. Various processing filters from the VTK library created a 3D lower limb model from the ultrasound image dataset. However, the limitations presented by the quality of the ultrasound imaging technique contributed to initial problems in creating a 3D representation of a amputee's residual limb. To create a lower limb model that clearly showed the skin and bone contours, VTK used the segmented dataset to generate the surface polygons. The enhanced 2D Bayesian algorithm was selected to segment the entire ultrasound dataset based on its performance as discussed in the previous chapter. Then the filter classes diagramed in Figure 19 were used to generate a realistic 3D lower limb model of the outer skin and bone contours. After creating a realistic 3D lower limb model, the surface polygons were written to a file in a MOVIE.BYU format. Any application supporting MOVIE.BYU files can import the 3D lower limb model.
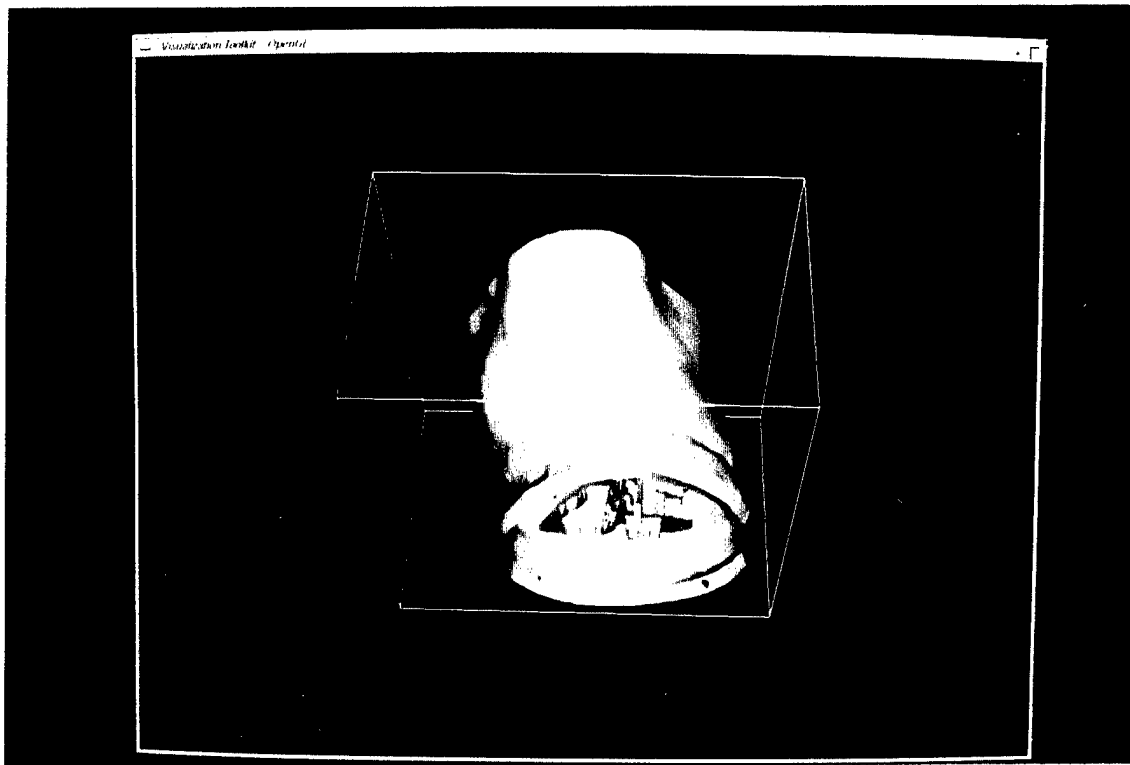
Figure 22 3D Model of Lower Limb with Smooth Outer Contour

6 Conclusion and Recommendations

Ultrasound imaging is quickly gaining popularity because it is efficient, inexpensive, and non-invasive [NELS93]. However, to produce rendered images that have the high quality of other modalities, more research is needed to develop faster, more accurate techniques that meet the special challenges poised by the unique low-noise ultrasound images described in Chapter 2. Even with image processing techniques, problems associated with noise, incomplete boundaries, and wide intensity variations within images still present obstacles for segmentation and creation of an accurate 3D lower limb model. These limitations are never completely eliminated during image processing since the goal is to optimize image quality while preserving important details.

Segmentation is very important for creating accurate models for use with a CASD system. My research identified and evaluated four potential segmentation techniques and enhancements that can be used to segment low-noise ultrasound residual limb images. I developed object-oriented C++ code or MATLAB code to test each segmentation algorithm. I also used the Visualization Toolkit to generate a realistic 3D model based on the segmented image dataset for use in a computer-aided socket design system.

Although this research was partially focused on segmenting the outer skin contour, which was done without difficulty, the important research dealt with the extraction of the bone structures. The enhanced 2D Bayesian algorithm produced fairly accurate segmentation of the lower limb. Dr. Ping He and Dr. Kefu Xue, two biomedical experts from Wright State University, verified the accuracy of segmentation of the tibia, the larger bone. Dr. He stated that for prosthetic socket design, the location of the tibia is the most important since it tends to bear most of the weight and requires relief areas. The fibula, the smaller bone, was much harder to distinguish due to the lack of boundary definitions from the tibia's backshadow. The fibula also needs accurate segmentation because prosthetists may need to know of its interaction

48

with the skin and tibia. Therefore, more research is need to overcome the difficulties inherent in ultrasound imaging to accurately extract the smaller bone region. The 3D Bayesian algorithm did not produce more accurate results than the enhanced 2D Bayesian and processed each slice slower than the 2D approach. Although the Marr-Hildreth algorithm was slightly faster, the its accuracy was also less than that of the 2D Bayesian.

Segmentation may be improved by creating a model-driven approach, such as the genetic algorithm technique presented by Heckman and Krumm. This type of approach could help offset the distractions caused by noise since their GA was able to produce accurate segmentation of both regions. However, Heckman and Krumm's technique is not automated and relies on some human interaction for locating bounding boxes of the bone structures. Although this step could be automated using the 2D Bayesian algorithm to extract the bounding boxes, this additional step would increase the overhead. The genetic algorithm is quite slow compared to the other algorithms since it covers a huge search space and adding the extra step to automate segmentation would further decrease speed. Furthermore, each execution of the algorithm produces different results since the genetic algorithm is based on finding an optimal solution not the best one.

Overall, for quick speed and relative accuracy the enhanced 2D Bayesian produced the best segmentation of ultrasound images. However, further work is required to increase accuracy in the segmentation of the two bones especially the fibula. Future success may result from trying to incorporate and mimic the human perceptual system and expert knowledge of ultrasound specialist and prosthetists.

Since the scope of this research focused primarily on segmentation, the improvement of surface tracking techniques was not researched in great detail. However, if increased speed is important, faster surface tracking could result by modifying the "marching cubes" algorithm in the VTK library. The algorithm could be enhanced by using the approach proposed by Livnat, *et al.* Unlike the "marching cubes" algorithm which inspects each and every voxel to see if a

surface intersects it, their near-optimal isosurface extraction (NOISE) algorithm, a faster technique released in March 1996, uses a multidimensional binary tree structure to quickly eliminate voxels that do not meet the criteria for being intersected. As a result, the algorithm is faster and more efficient in identifying the voxels that have surfaces cutting through them [LIVN96].

In addition, the primary concern of my research was on the evaluation of various segmentation techniques on specialized ultrasound images. Therefore, I mainly concentrated on fast implementation of the different algorithms and did not emphasize speed and efficiency of processing. Therefore, my implementation of the different segmentation techniques may need further analysis for modifications leading to faster processing and lower memory requirements.

With further research and improvements on the work presented here, a more realistic and accurate model of the residual limb of a BK amputee could be created to help solve the problems that exist with conventional prosthetic socket design which would save money, provide greater comfort, and more mobility to amputees.

Bibliography

[ASHT94A]   Ashton, Edward A. and Keven J. Parker. "Multiple Resolution Bayesian Segmentation of Ultrasound Images," *SPIE Visualization in Biomedical Computing*, 2359, October 1994, pp. 38-49.

[ASHT94B]   Ashton, Edward A., Michel J. Berg, and Kevin J. Parker. "Segmentation and Features Extraction Techniques, with Applications to Biomedical Images," *IEEE International Conference on Image Processing*, November 1994, pp. 726-30.

[ASHT95A]   Ashton, Edward A. and Kevin J. Parker. "Multiple Resolution Bayesian Segmentation of Ultrasound Images," *Ultrasonic Imaging*, 17(4), October 1995, pp. 291-304.

[ASHT95B]   Ashton, Edward A.; Michel J. Berg; Kevin J. Parker; Jeffrey Weisberg; Change Wen Chen; and Leena Ketonen. "Segmentation and Feature Extractio Techniques, with Applications to MRI Head Studies," Magnetic Resonance in Medicine: Official Journal of the Society of Magnetic Resonance in Medicine, 33(5), May 95, pp. 670-77.

[BARI93]   Barillot, Christian. "Surface And Volume Rendering Techniques To Display 3-D Data," *IEEE Engineering in Medicine and Biology*, 12(1), March 1993, pp. 111-119.

[BESA86]   Besag, J. "On the Statistical Analysis of Dirty Pictures," *Journal of the Royal Statistical Society*, 48(3), 1986, pp. 259-302.

[BEZD93]   Bezdek, J. C.; L. O. Hall; and L. P. Clarke. "Review of MR Image Segmentation Techniques Using Pattern Recognition," *Medical Physics*, 20(4), July/August 1993, pp. 1033-1048.

[BOMA90]   Bomans, M.; K.-H. Hohne; U. Tiede; and M. Riemer. "3D Segmentation of MR Images of the Head for 3D Display," *IEEE Transactions on Medical Imaging*, 9(2), June 1990, pp. 177-183.

[CAST96]   Castleman, Kenneth. *Digital Image Processing*, Englewood Cliffs, N. J.: Prentice Hall, 1996.

[CHAN93]   Chang, Michael M.; A. Murat Tekalp; and M. Ibrahim Sezan. "Bayesian Segmentation of MR Images Using 3D Gibbsian Priors," *SPIE Conference on Image and Video Processing*, 1903, February 1993, pp. 122-131.

[CIBA87]   "Musculoskeletal System. Part I, Anatomy, Physiology and Metabolic Disorders", ed. Frank Netter, *The CIBA Collection of Medical Illustrations*, 8(1), West Caldwell, N.J.: CIBA Medical Education Division, 1987.

[CLAR95]   Clarke, L. P., *et al.* " MRI Segmentation: Methods and Applications," *Magnetic Resonance Imaging*, 13(3), 1995, pp. 343-368.

[ENGS92]   Engsberg, J. R., *et al.* "A CAD CAM Method for Custom Below-Knee Sockets," *Prosthetics and Orthotics International*, 16(3), December 1992, pp. 183-188.

[HE94]   He, P. and K. Xue. "A PC-Based Ultrasound Scanning System for Imaging a Residual Limb,"*Proceedings of the 16th Annual International Conference of the IEEE Engineering in Medicine and Biology Society*, November 1994, pp. 480-481.

[HE96]   He, Ping; Kefu Xue; Qun Chen; Paul Murka; and Scott Schall. "A PC-Based Ultrasonic Data Acquisition System for Computer-Aided Prosthetic Socket Design," *IEEE Transactions on Rehabilitation Engineering*, 4(2), June 1996, pp. 114-119.

[HECK96]   Heckman, Tom and John Krumm. "Searching for Contours," *SPIE Image and Video Processing IV*, 2666, February 1996, pp. 223-232.

[HERM90]   Herman, Gabor T. "A Survey of 3D Medical Imaging Technologies," *IEEE Engineering in Medicine and Biology*, ??, December 1990, pp. 15 -17.

[HOUS92]   Houston, Vern L.; et al. "Auuutomated Fabrication of Mobility Aids (AFMA): Below-knee CASD/CAM testing and evaluation program results," Journal of Rehabilitation and Development, 29(4), 1992, pp. 78-124.

[LIN91]   Lin, W. J., S. W. Pizer, and V. E. Johnson. "Boundary Estimation in Ultrasound Images," Lecture Notes in Computer Science, *Proceedings of Information Processing in Medical Imaging: Twelfth International Conference, IPMI '91*, Wye, U.K., 7-12 July 1991, pp. 285-299.

[LIVN96]   Livnat, Yarden; Han-Wei Shen, and Christopher R. Johnson. "A Near Optimal Isosurface Extraction Algorithm Using the Span Space," *IEEE Transactions on Visualization and Computer Graphics*, 2(1), March 1996, pp. 73-84.

[LORE87]   Lorensen, William E. and Harvey E. Cline. "Marching Cubes: A High Resolution 3D Surface Construction Algorithm," *ACM Computer Graphics*, 21(24), July 1987, pp. 163-169.

[LYBA94]   Lybanon, Matthew; Suzanne M. Lea; and Susam M. Himes. "Segmentation of Diverse Image Types Using Opening and Closing,"

IEEE Proceedings of the 12th IAPR International Conference on Pattern Recognition, October 1994, pp. 347-351.

[MORI95]   Morimoto, Alan K.; et al. "3D Ultrasound Imaging for Prothesis Fabrication and Diagnostic Imaging," *SANDIA REPORT*, SAND94-3137, June 1995.

[NELS93]   Nelson, Thomas R. and T. Todd Elvins. "Visualization of 3D Ultrasound Data," *IEEE Computer Graphics and Applications*, 13(6), November 1993, pp. 50-57.

[PAPP92]   Pappas, Thrasyvoulos N. "An Adaptive Clustering Algorithm for Image Segmentation," *IEEE Transaction on Signal Processing*, 40(4), April 1992, pp. 901-914.

[PAVL82]   Pavlidis, Theo. *Algorithms for Graphics and Image Processing*, Rockville, M.D.: Computer Science Press, 1982.

[SAKA95A]   Sakas, Georgios and Stefan Walter. "Extracting Surfaces from Fuzzy 3D-Ultrasound Data," *ACM SIGGRAPH Conference Proceedings*, August 6 - 11 1995, pp. 465-474.

[SAKA95B]   Sakas, Georgios; Lars-Arne Schreyer; and Marcus Grimm. "Preprocessing and Volume Rendering of 3D Ultrasonic Data," *IEEE Computer Graphics and Applications*, July 1995, pp. 47-54.

[SAND86]   Sanders, Gloria T. *Lower Limb Amputations: A Guide To Rehabilitation*, Philadelphia: F. A. Davis Co., 1986.

[SCHR96]   Schroeder, Will; Martin, Ken; and Bill Lorenson. *The Visualization Toolket: An Objected-Oriented Approach To 3D Graphics*, Upper Saddle River, N.J.: Prentice Hall PTR, 1996.

[SMIT95]   Smith, Kirk E.; Michael W. Vannier; and Paul K. Commean. "Spiral CT Volumetry of Below-knee Residua," *IEEE Transactions on Rehabilitation Engineering*, 3(3), September 1995, pp. 235-241.

[STYT90]   Stytz, M. R. and O. Frieder. "Three-Dimensional Medical Imaging Modalities: An Overview," *Critical Reviews in Biomedical Engineering*, 18(1), 1990, pp. 27-54.

[STYT91]   Stytz, M. R., G. Frieder and O. Frieder. "Three-Dimensional Medical Imaging: Algorithms and Computer Systems." *ACM Computing Surveys*, 23(4), December 1991, pp. 421-499.

[THOM91]   Thomas, Judith G.; Richard Alan Peters; and Philippe Jeanty. "Automatic Segmentation of Ultrasound Images Using Morphological

Operators," *IEEE Transactions on Medical Imaging*, 10(2), June 1991, pp.180-186.

[TOPP90]   Topper, A. K. and G. R. Fernie., "An Evaluation of CAD of Below-knee Prosthetic Sockets," *Prosthetics and Orthotics International*, 14(3), December 1990, pp. 136-142.

[UDUP90]   Udupa, Jayaram K. and Hsiu-Mei Hung. "Surface Versus Volume Rendering: A Comparative Assessment," *Proceedings of First Conference on Visualization in Biomedical Computing*, May 1990, pp. 83-91.

[UDUP91]   Udupa, Jayaram K. "Computer Aspects of 3D Imaging in Medicine: A Tutorial," *3D Imaging in Medicine*, Boca Raton, FL: CRC Press, 1991, pp. 1-85.

[XUE91]   Xue, Kefu; Ping He; Huimin Fu; Hisham A. Bismar. "An Ultrasonic B-Scan Image Compounding Technique For Prosthetic Socket Design," SPIE Visual Communications and Image Processing '91, 1606, pp. 675-684.

[YAN94]   Yan, Michelle X.H. and Joel S. Karp. "Segmentation of 3D Brain MR Using An Adaptive K-means Clustering Algorithm," *IEEE 1994 Nuclear Science Symposium and Medical Imaging Conference*, 4, pp. 1529-1533.

Appendix A: Original Ultrasound Images Slices
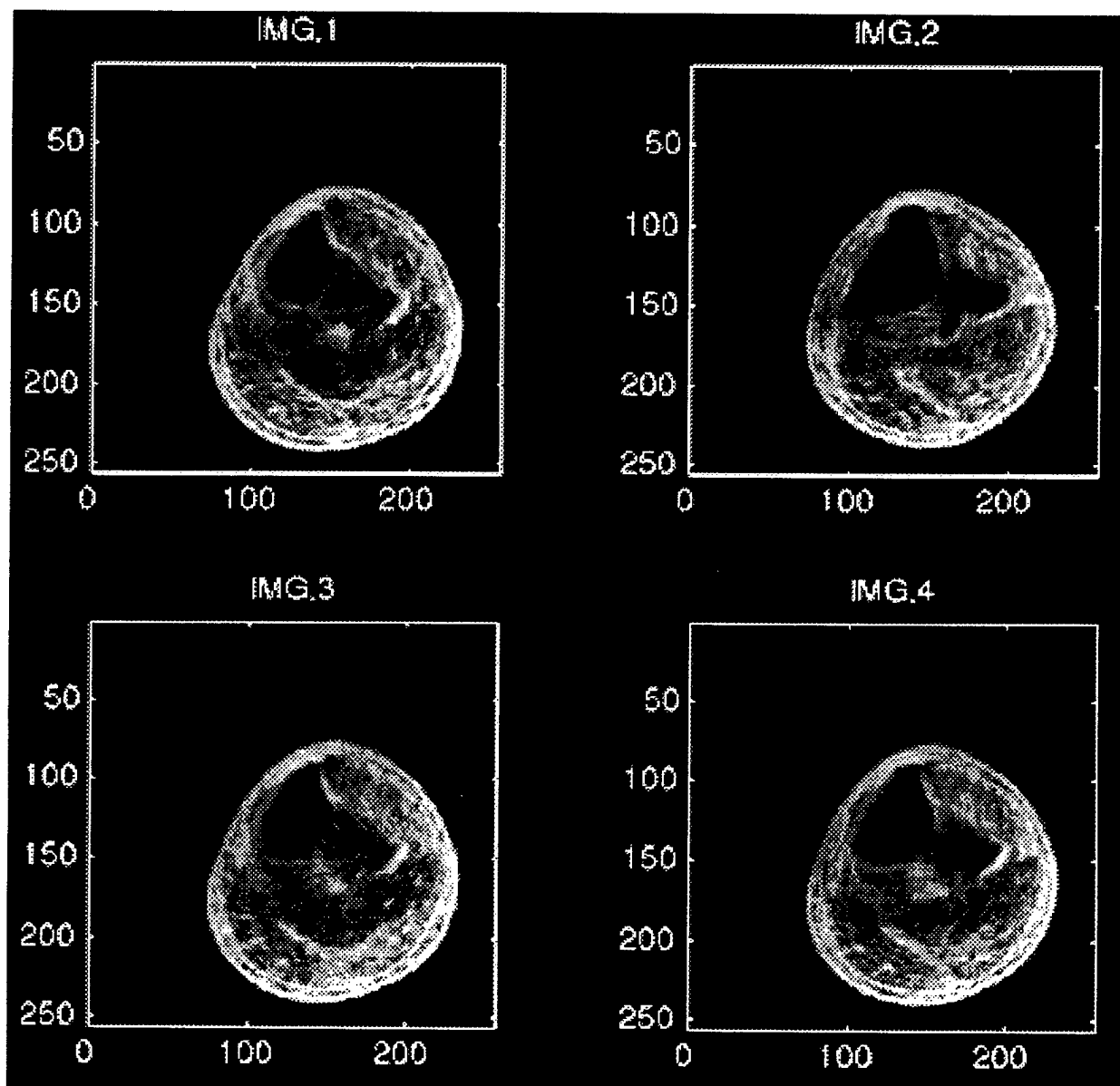
Ultrasound Image Slices 1 - 4 of 3D Dataset
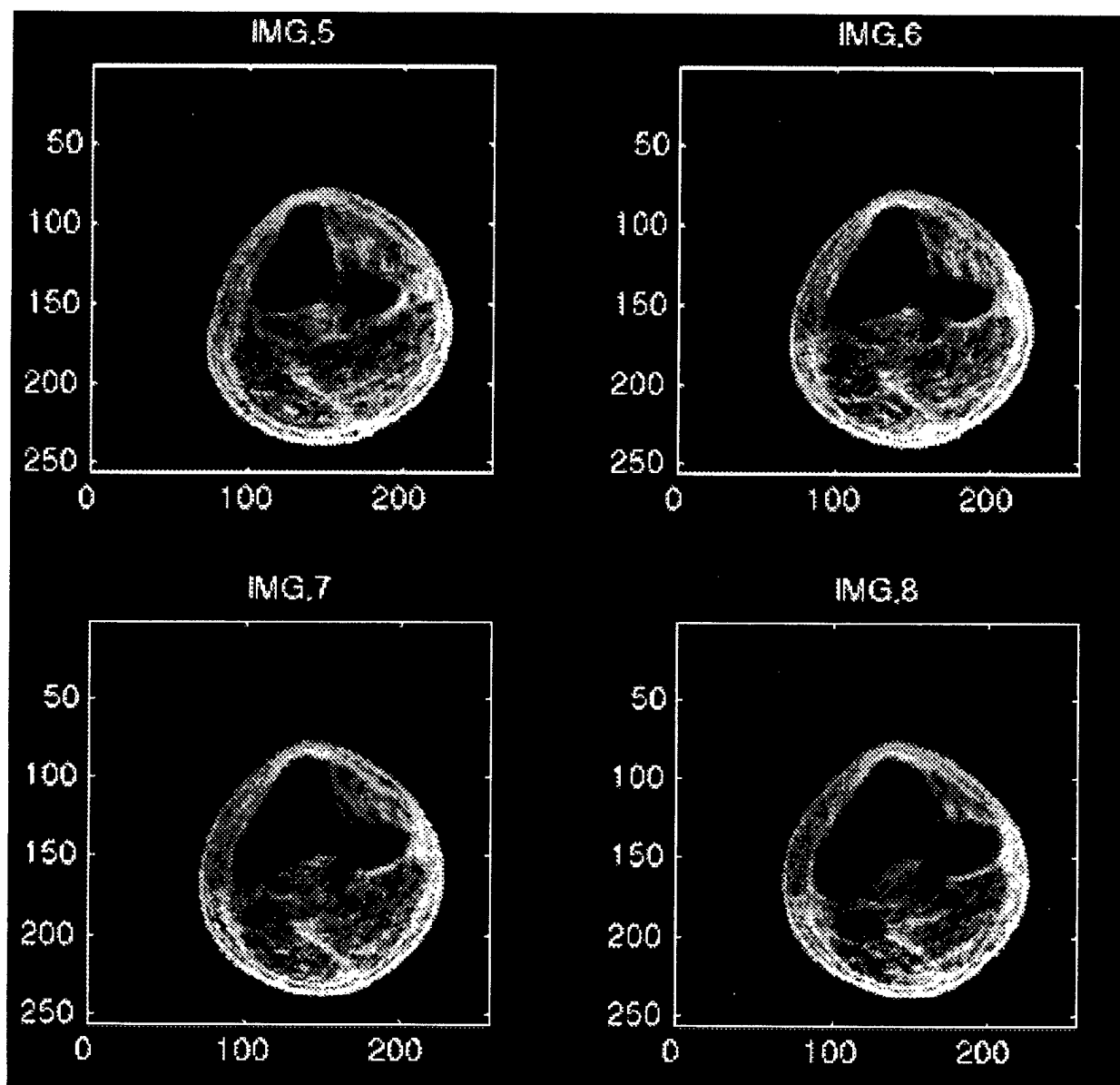
Ultrasound Image Slices 5 - 8 of 3D Dataset
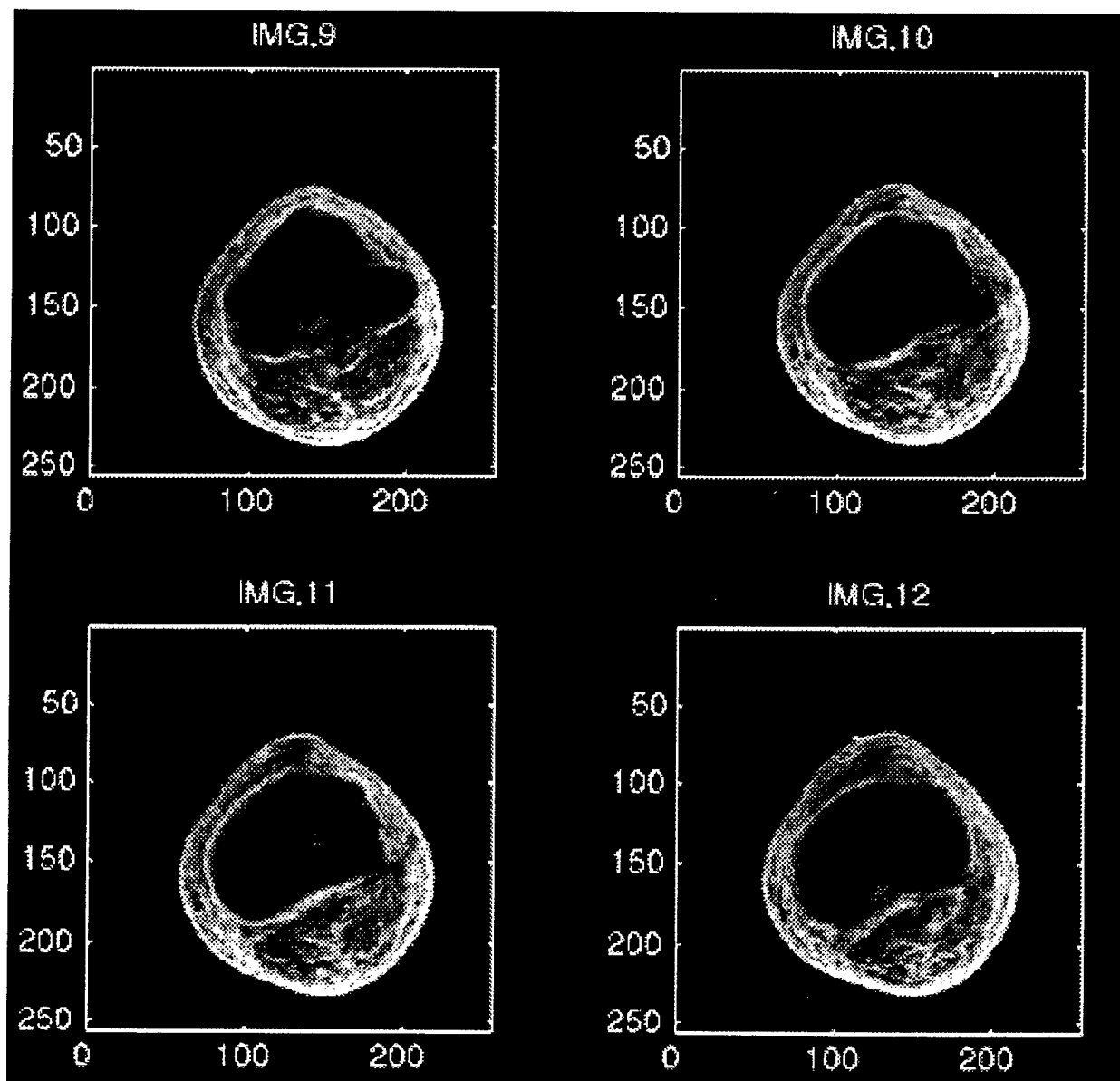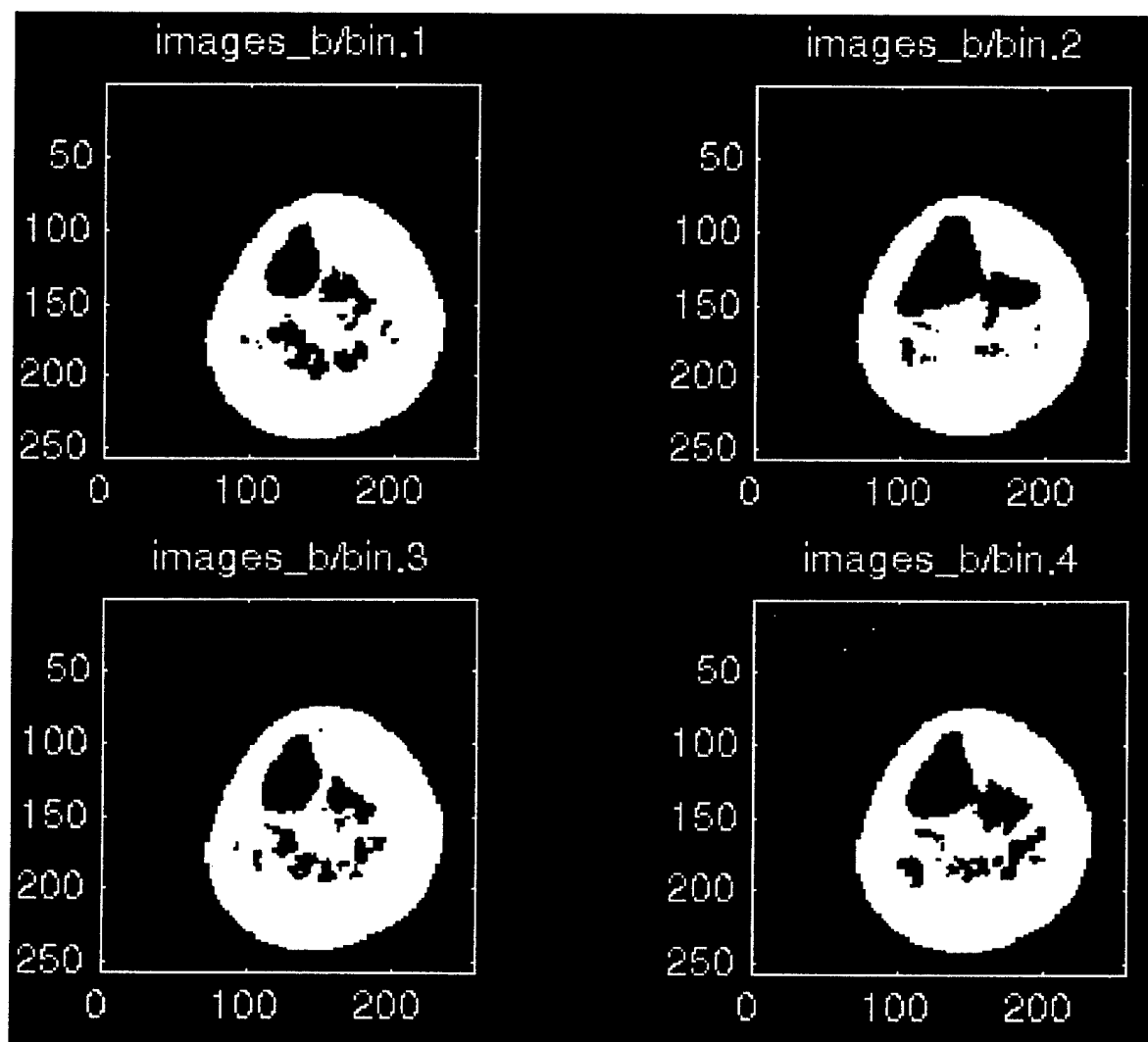
Ultrasound Image Slices 9 - 12 of 3D Dataset
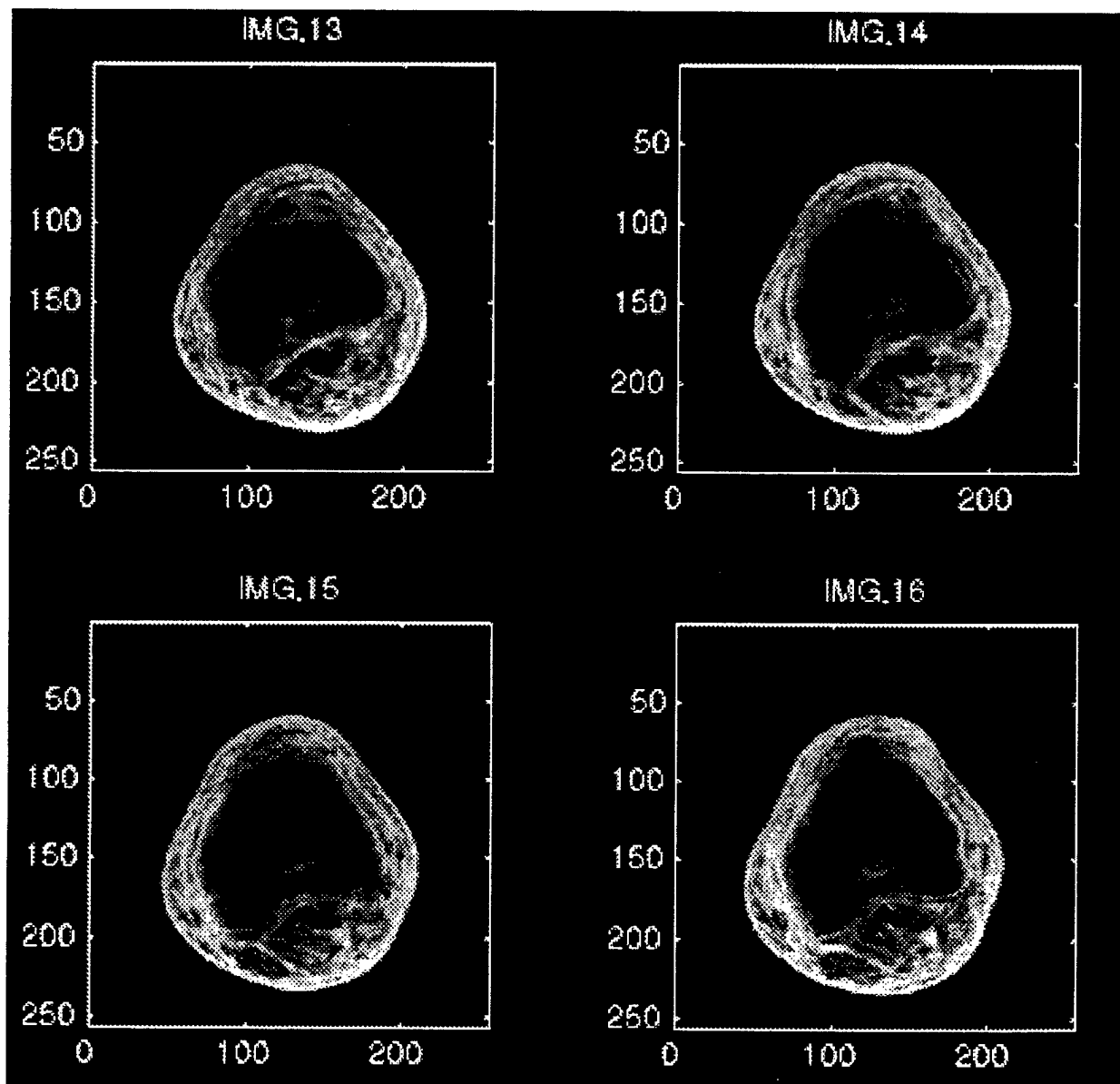
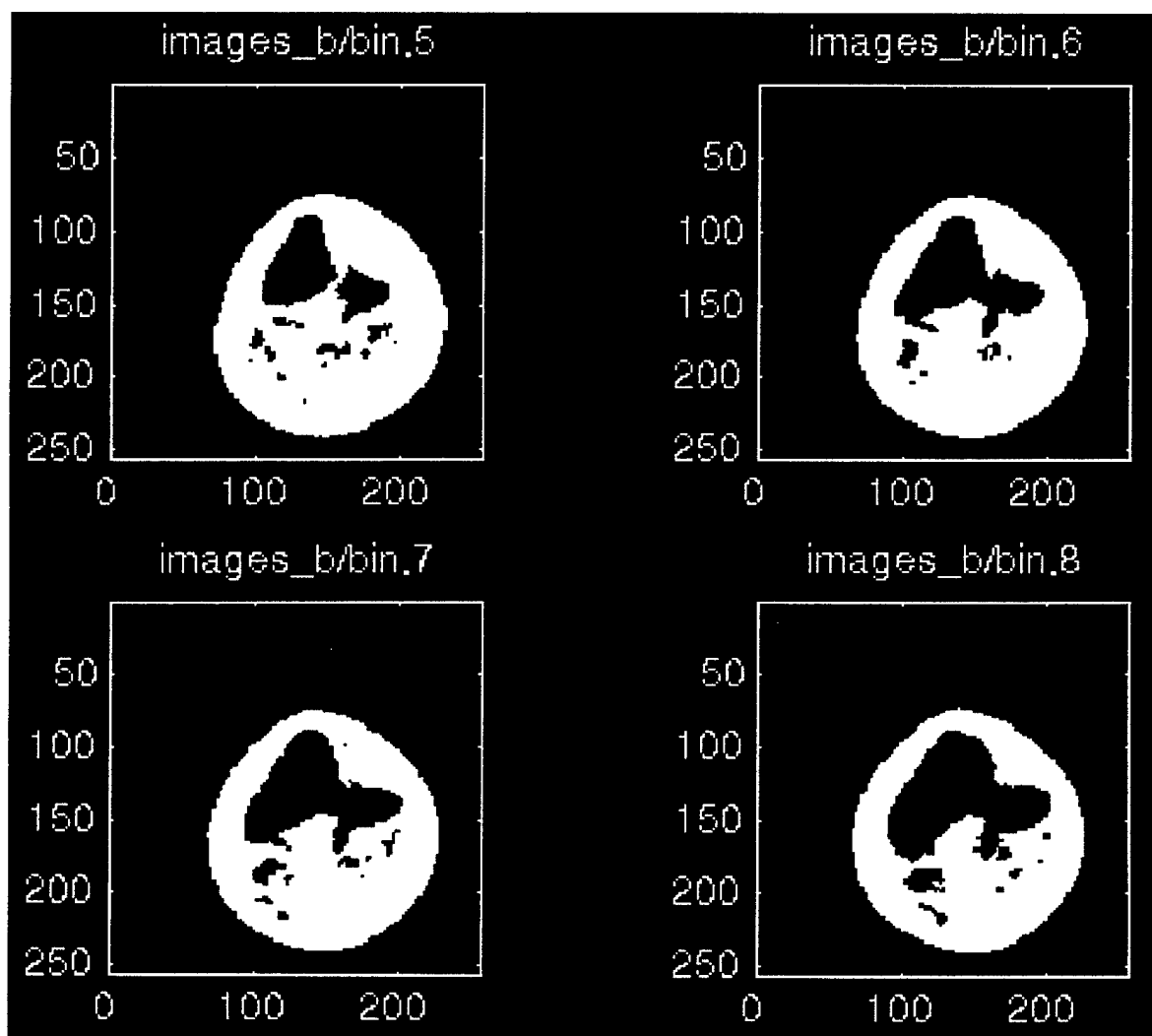Ultrasound Image Slices 13 - 16 of 3D Dataset
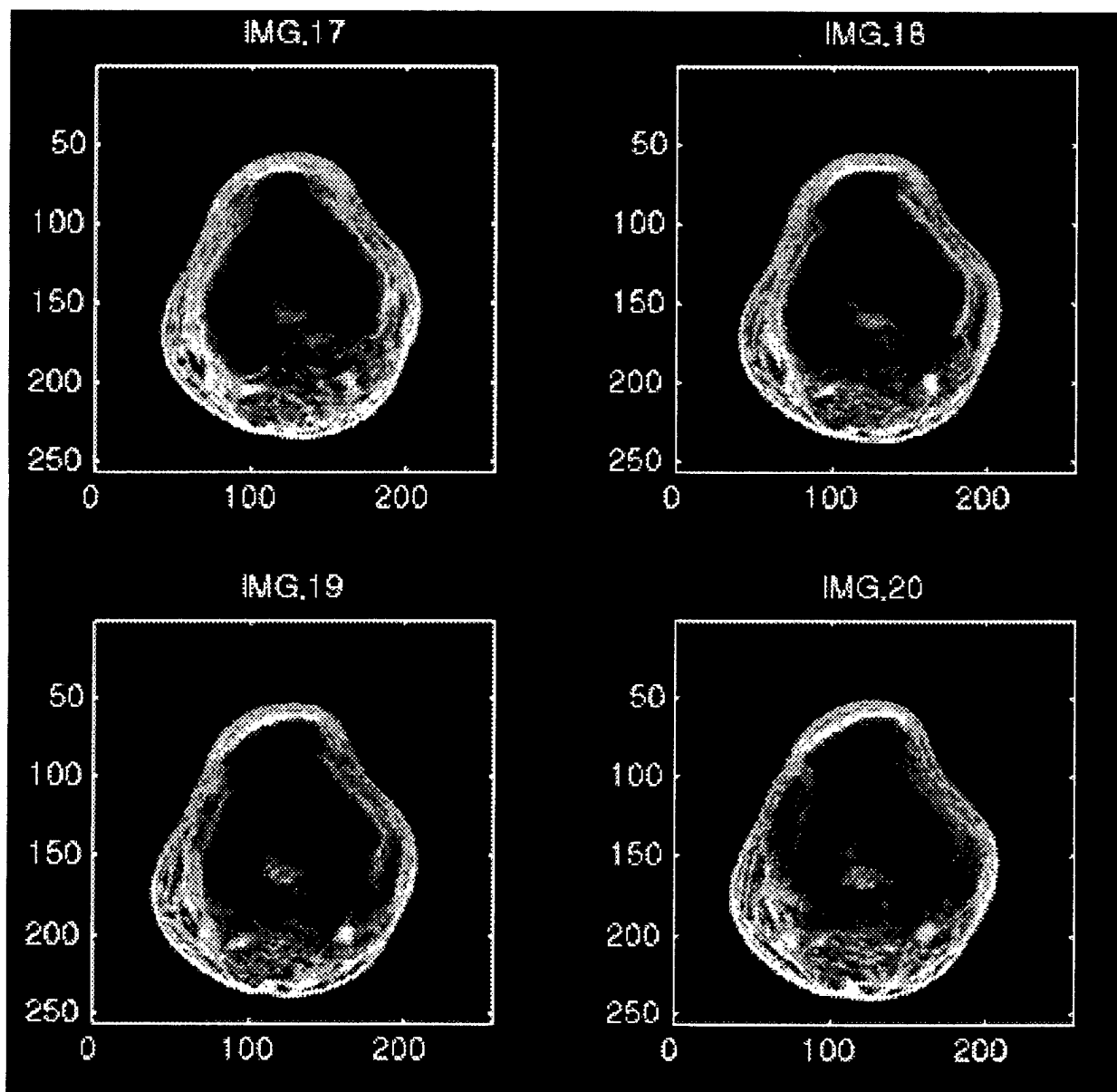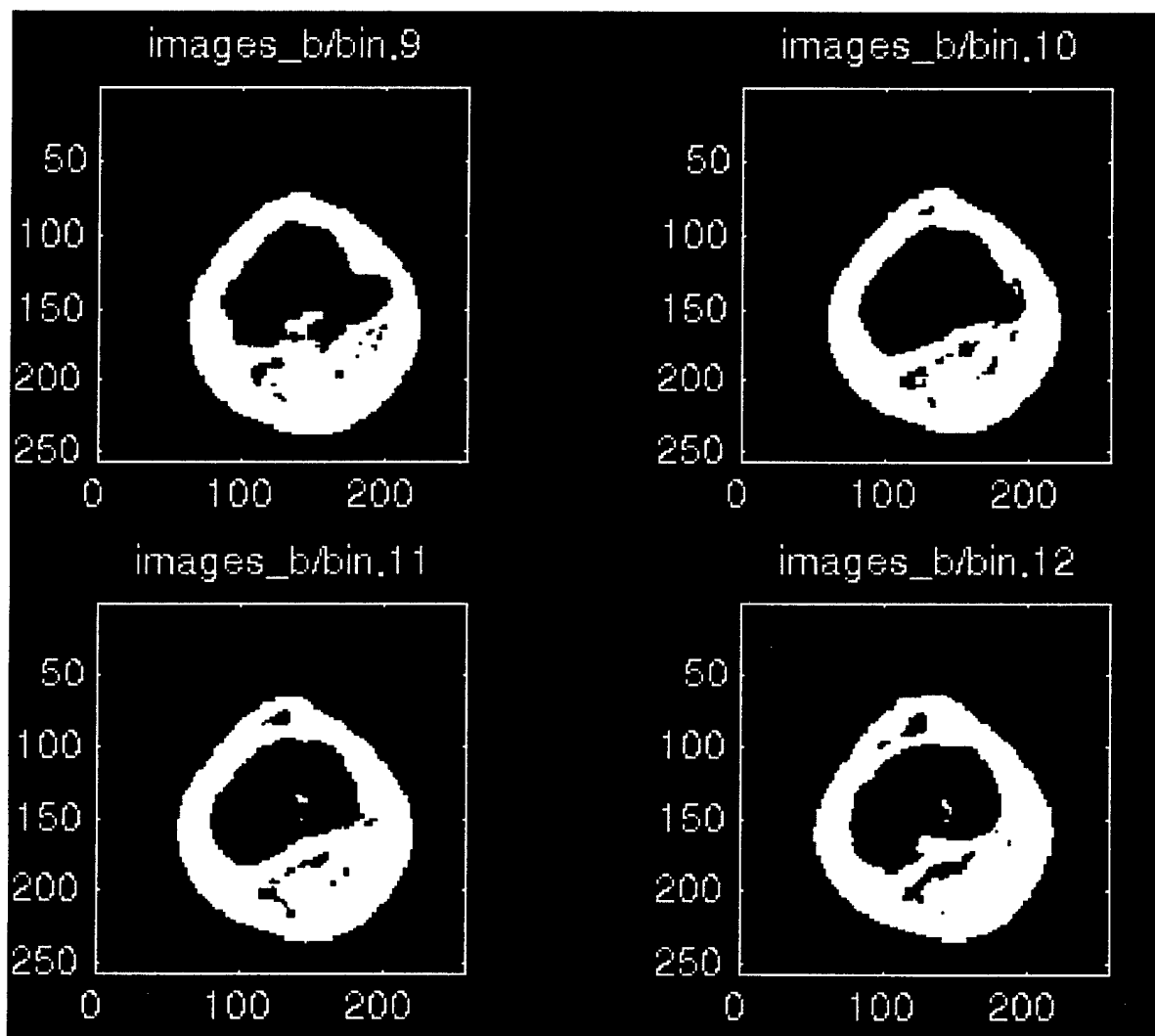
Ultrasound Image Slices 17 - 20 of 3D Dataset

Appendix B: 2D Bayesian Segmented Images

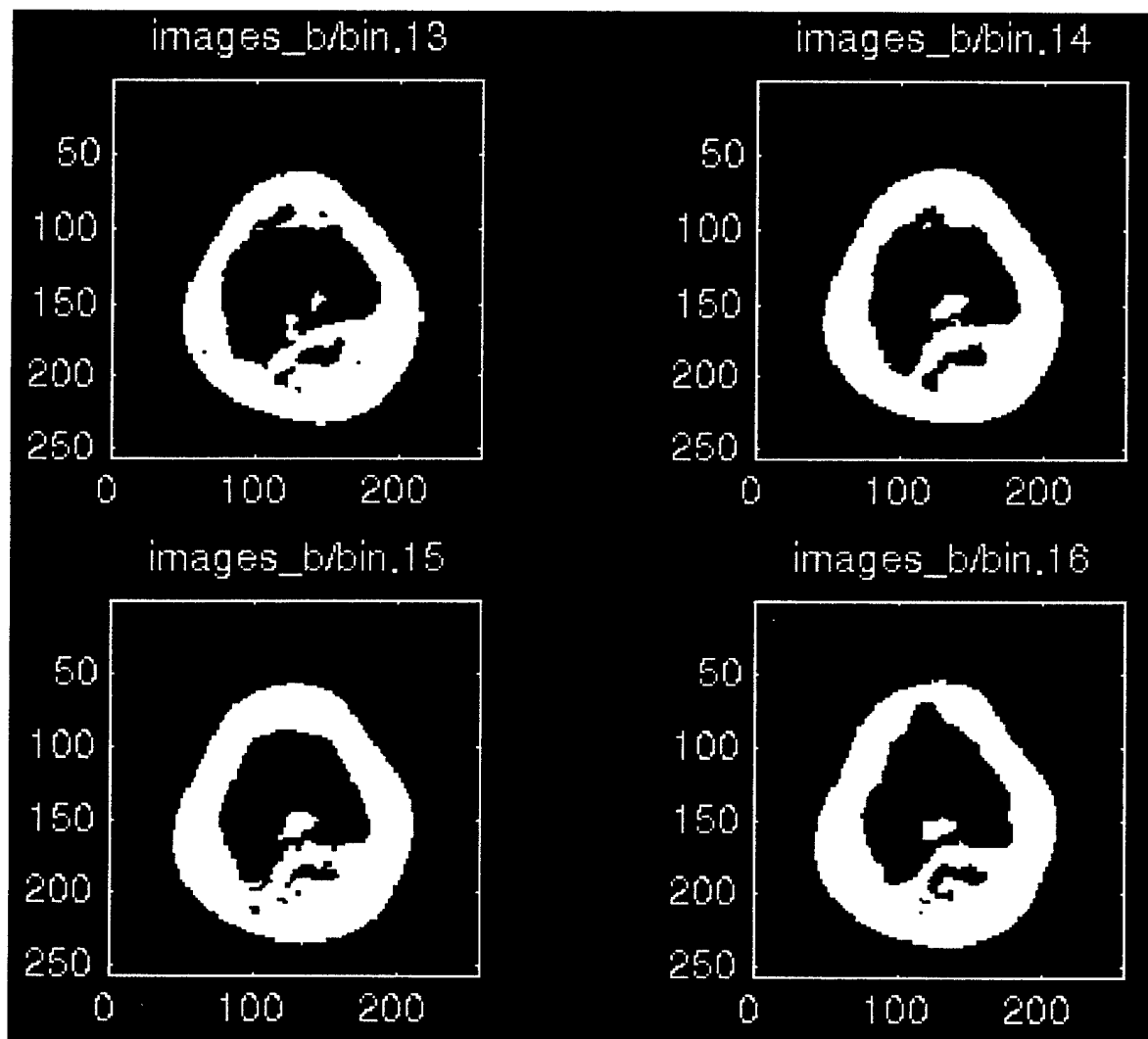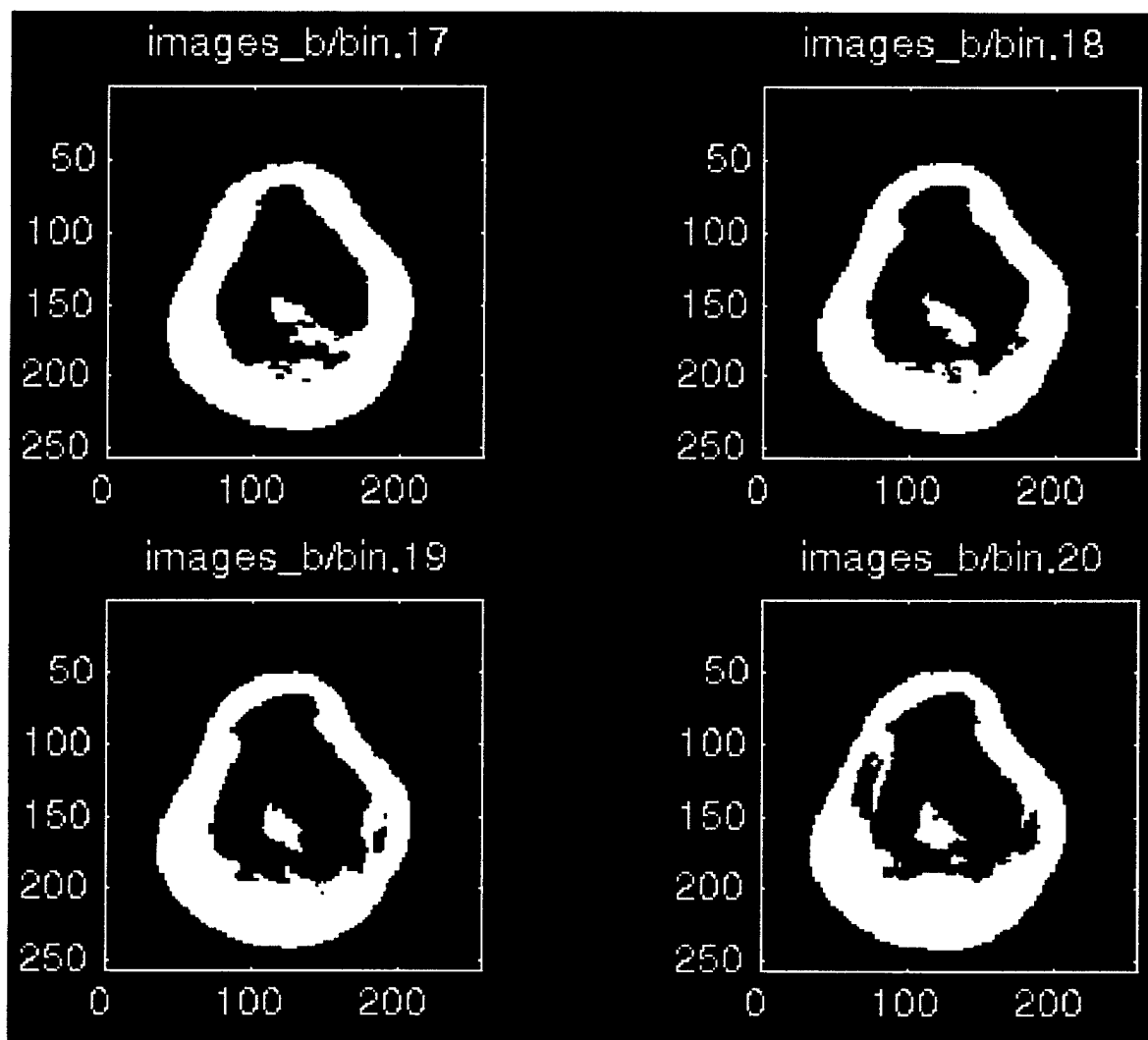Ultrasound Segmented Slices 1 - 4 of 3D Dataset

Ultrasound Segmented Slices 5 - 8 of 3D Dataset

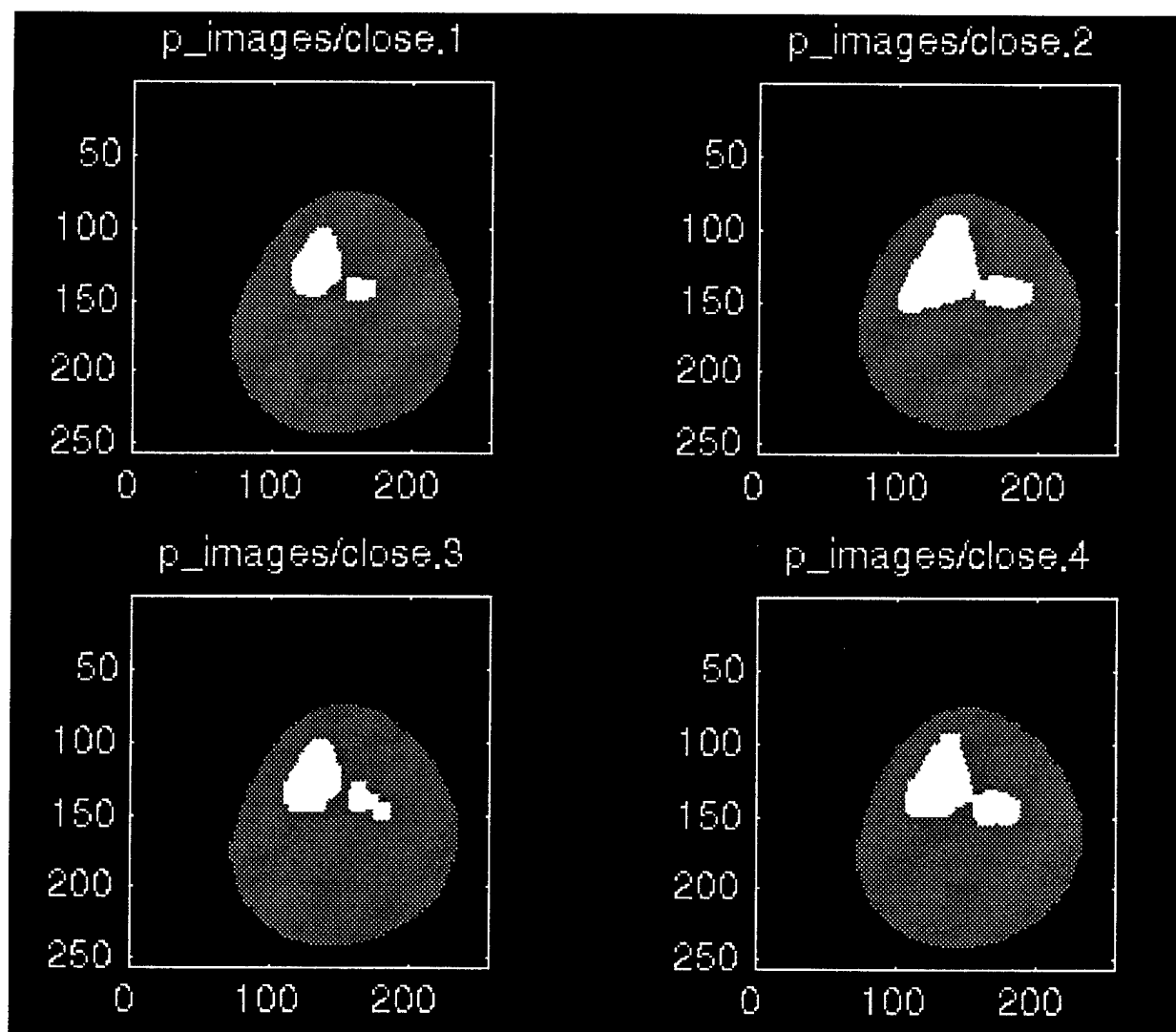Ultrasound Segmented Slices 9 - 12 of 3D Dataset

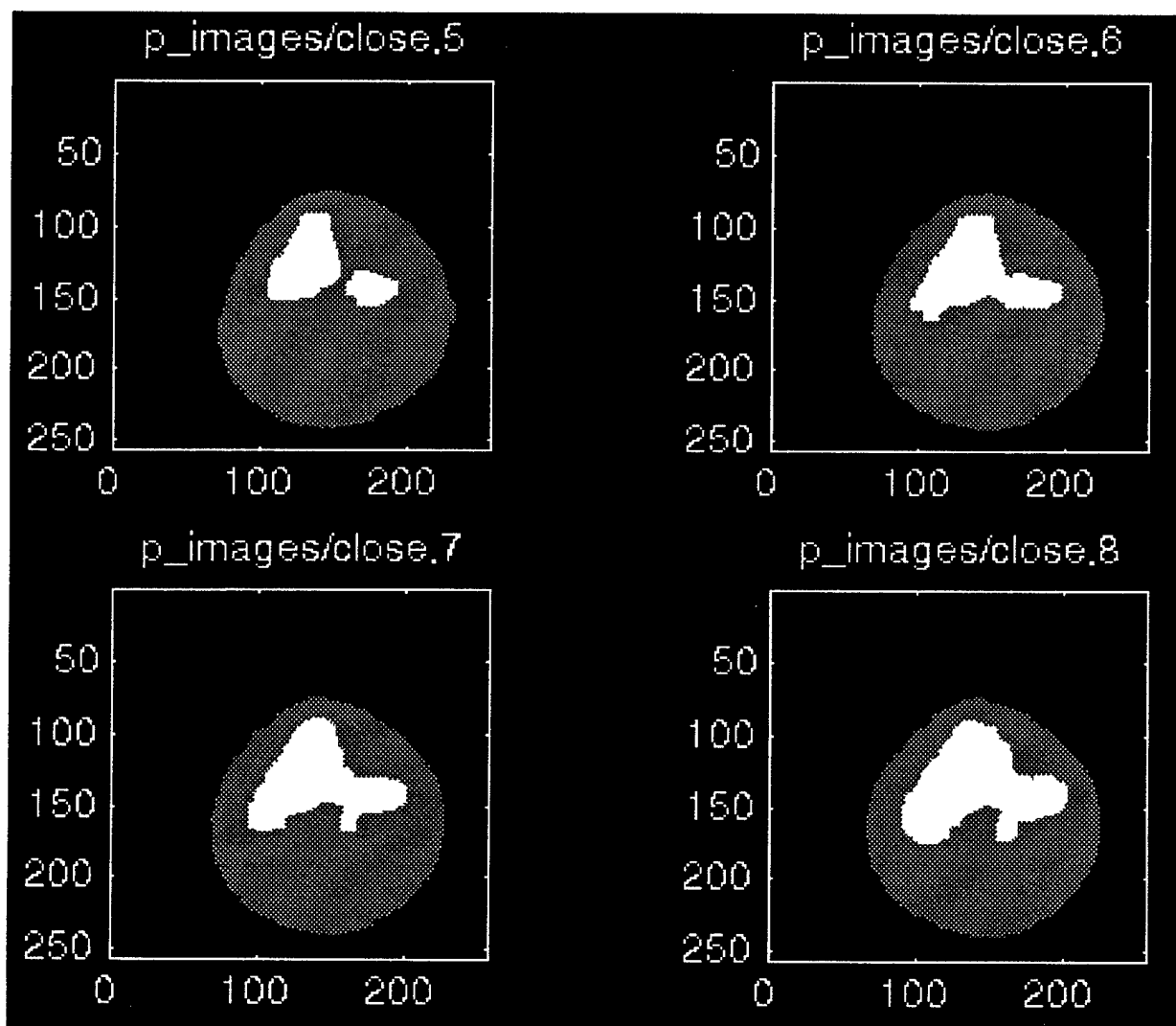Ultrasound Segmented Slices 13 - 16 of 3D Dataset

63

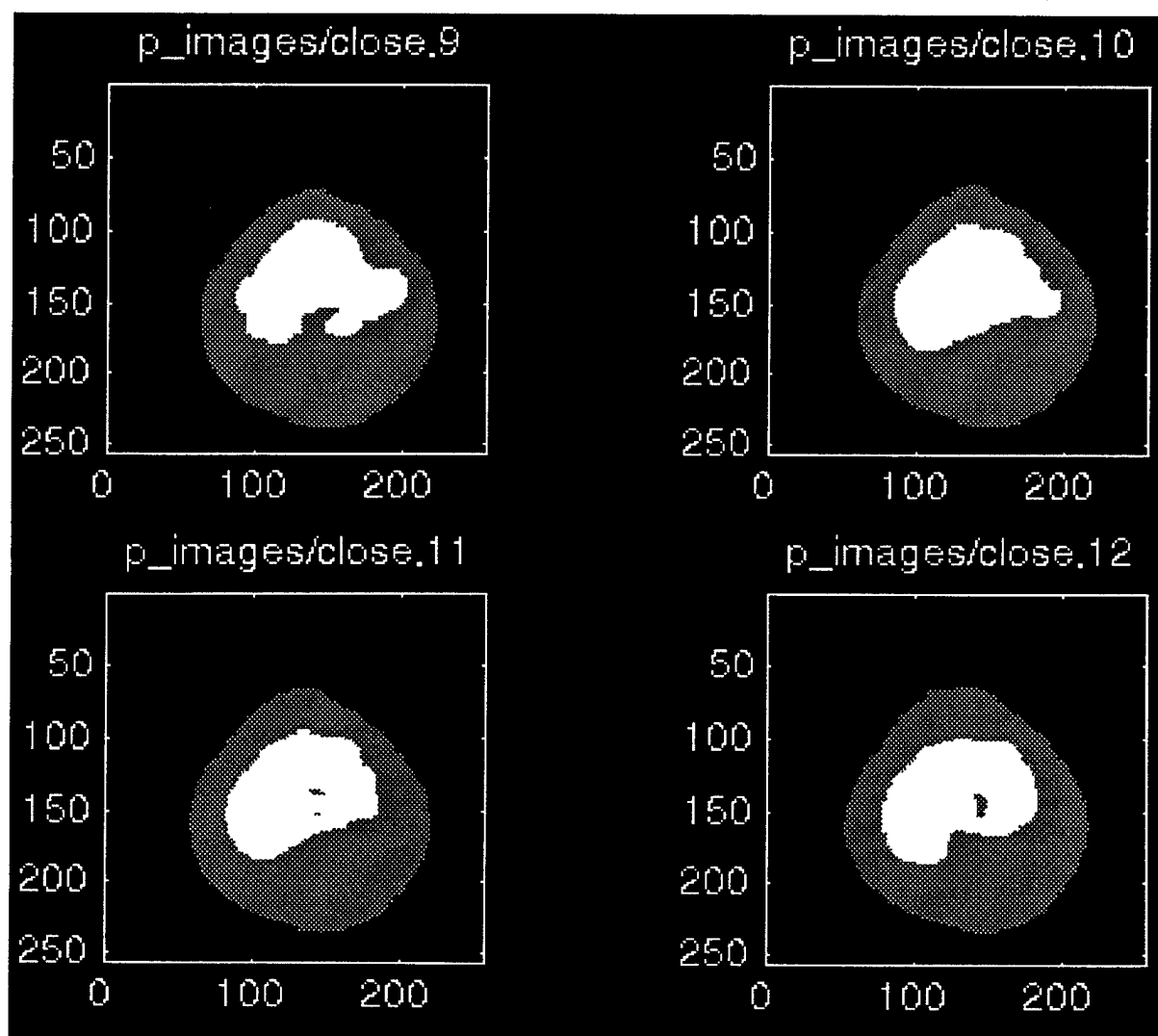Ultrasound Segmented Slices 17 - 20 of 3D Dataset

64

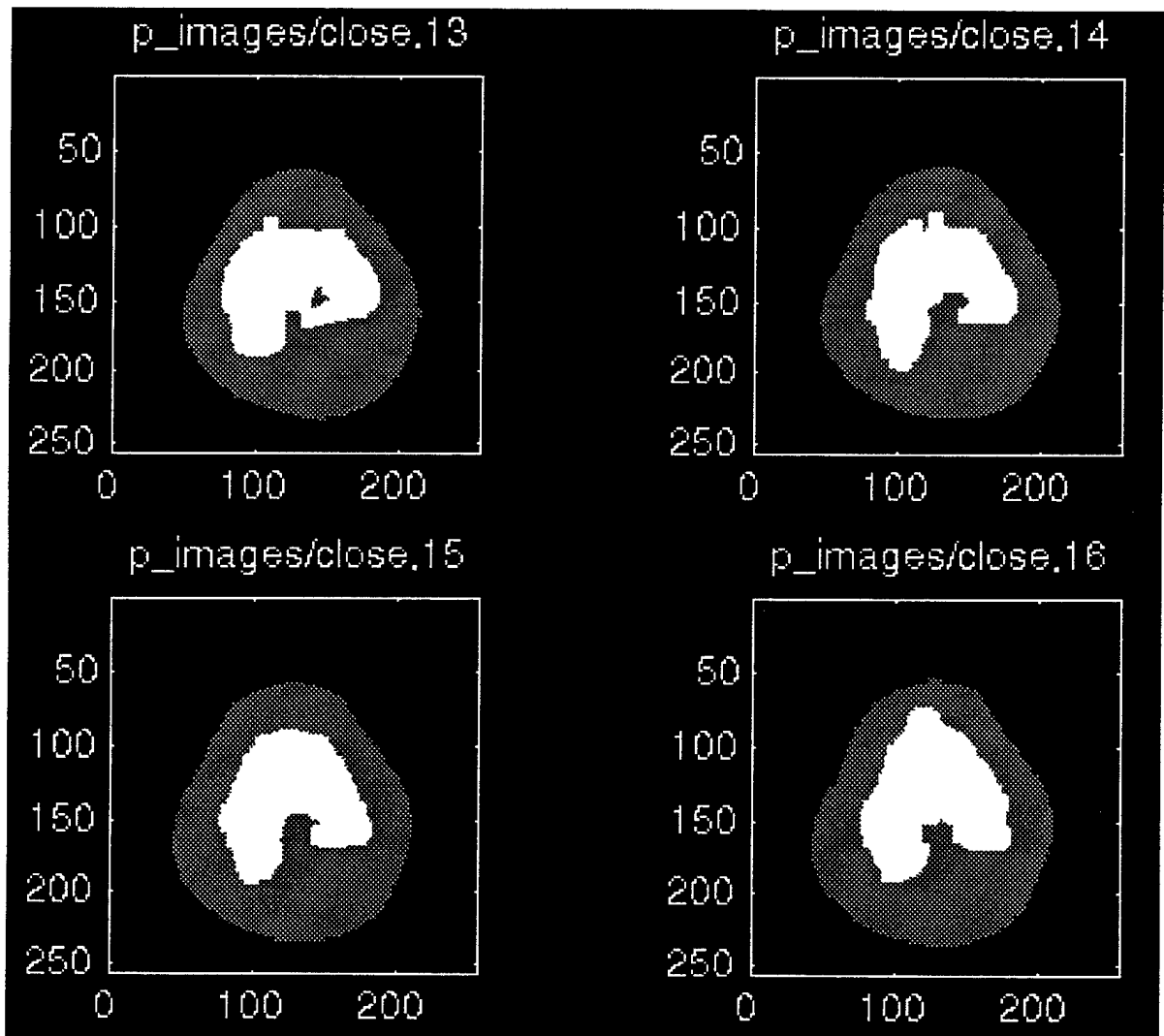# Appendix C: Enhanced 2D Bayesian Segmented Images

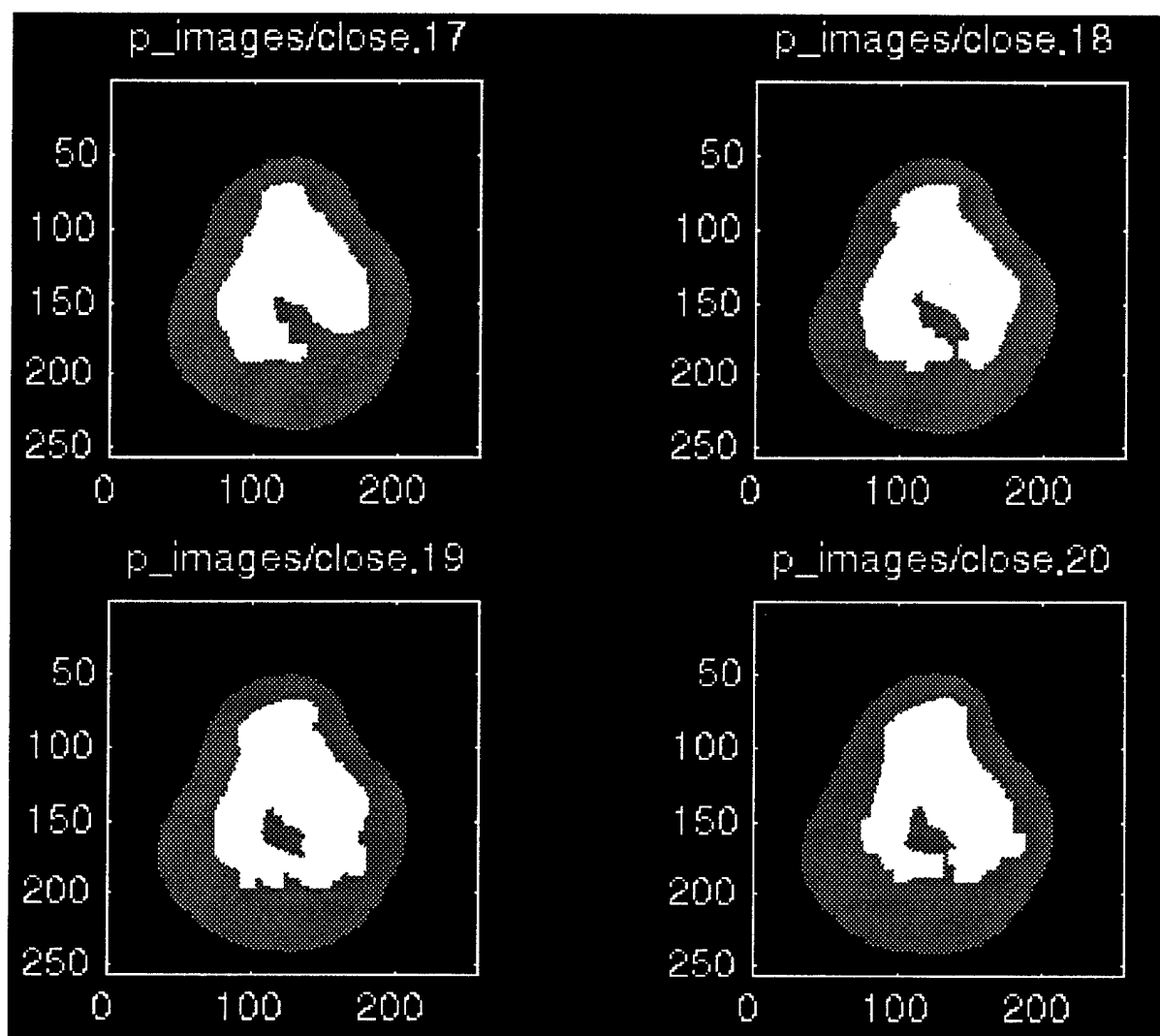Ultrasound Segmented Slices 1 - 4 of 3D Dataset

Ultrasound Segmented Slices 5 - 8 of 3D Dataset

66

Ultrasound Segmented Slices 9 - 12 of 3D Dataset

Ultrasound Segmented Slices 13 - 16 of 3D Dataset

Ultrasound Segmented Slices 17 - 20 of 3D Dataset

Vita

First Lieutenant Min Cha Baker was born in Chun Chon, South Korea on 17 June 1971. She graduated from the University of North Carolina at Chapel Hill with a B.S. degree in Mathematical Sciences with special emphasis on Computer Science in May of 1993. After graduation, she was commissioned into the United States Air Force. Upon entering extended active duty, she was sent to Keesler AFB, Mississippi for Basic Communication Officer Training (BCOT). After completing BCOT, Lieutenant Baker's first assignment was at Tinker AFB, Oklahoma with the 38th Engineering Installation Wing's Software Directorate, where she started out testing flight systems software and then, later developed technical control software to support world-wide communications resources. In 1995, Lieutenant Baker married John Erick McNett, who is also an officer in the Air Force stationed at Wright Patterson AFB, Ohio. In June of 1995, she started a Master's program in Computer Systems at the Air Force Institute of Technology.

Permanent address: 3607 Kennington Drive
                     Waxhaw, North Carolina 28173

1. AGENCY USE ONLY *(Leave blank)*	2. REPORT DATE Dec 96	3. REPORT TYPE AND DATES COVERED Master's Thesis

4. TITLE AND SUBTITLE
EVALUATION OF SEGMENTATION FOR BONE STRUCTURES IN 3D RENDERING OF ULTRASOUND RESIDUAL LIMB IMAGES

5. FUNDING NUMBERS

6. AUTHOR(S)
1st Lt Min C. Baker, USAF

7. PERFORMING ORGANIZATION NAME(S) AND ADDRESS(ES)
Air Force Institute of Technology
2750 P Street
WPAFB, OH 45433-7765

8. PERFORMING ORGANIZATION REPORT NUMBER

AFIT/GCS/ENG/96D-03

9. SPONSORING/MONITORING AGENCY NAME(S) AND ADDRESS(ES)
Jennifer J. Whitestone
AL/CFHD, Bldg 248A
2255 H Street
WPAFB, OH 45433-7022

10. SPONSORING/MONITORING AGENCY REPORT NUMBER

11. SUPPLEMENTARY NOTES

12a. DISTRIBUTION AVAILABILITY STATEMENT
Approved for public release; Distribution unlimited

12b. DISTRIBUTION CODE

13. ABSTRACT *(Maximum 200 words)*
Prosthetists today widely practice manual socket fitting, which produces subjective, inconsistent results. To address this problem, the Computerized Anthropometry Research and Design (CARD) Laboratory is developing a computer-aided socket design system that acquires ultrasound datasets of an amputee's residual limb, creates a 3D model, and helps identify load-bearing and pressure-relief areas. This research project focuses on providing 3D visualization of a residual limb to support the CARD Laboratory's efforts. Creating the 3D model of the skin and two bone contours requires two major steps: segmentation to identify the objects of interest and a surface tracking algorithm to generate the polygonal database of the surface contours. Low-level noise, incomplete boundaries, and widely varying intensities within the images present a difficult challenge to segmentation as well as to the construction of a 3D model. Therefore, different techniques have been explored to achieve accurate segmentation and realistic 3D rendering of unique ultrasound images. Among various segmentation techniques tested, the enhanced 2D multiresolution Bayesian efficiently produces accurate segmentation of outer skin contour and bone locations of the lower limb. The basic technique applies a filter-and-decimate approach coupled with an adaptive clustering algorithm and is modified to use anatomical characteristics to detect and eliminate artifacts.

14. SUBJECT TERMS
Ultrasonics, Medical Imaging, Segmentation, Medical Computer Applications

15. NUMBER OF PAGES
77

16. PRICE CODE

17. SECURITY CLASSIFICATION OF REPORT	18. SECURITY CLASSIFICATION OF THIS PAGE	19. SECURITY CLASSIFICATION OF ABSTRACT	20. LIMITATION OF ABSTRACT
Unclassified	Unclassified	Unclassified	UL

GENERAL INSTRUCTIONS FOR COMPLETING SF 298

The Report Documentation Page (RDP) is used in announcing and cataloging reports. It is important that this information be consistent with the rest of the report, particularly the cover and title page. Instructions for filling in each block of the form follow. It is important to *stay within the lines* to meet *optical scanning requirements.*

Block 1. Agency Use Only *(Leave blank)*.

Block 2. Report Date. Full publication date including day, month, and year, if available (e.g. 1 Jan 88). Must cite at least the year.

Block 3. Type of Report and Dates Covered. State whether report is interim, final, etc. If applicable, enter inclusive report dates (e.g. 10 Jun 87 - 30 Jun 88).

Block 4. Title and Subtitle. A title is taken from the part of the report that provides the most meaningful and complete information. When a report is prepared in more than one volume, repeat the primary title, add volume number, and include subtitle for the specific volume. On classified documents enter the title classification in parentheses.

Block 5. Funding Numbers. To include contract and grant numbers; may include program element number(s), project number(s), task number(s), and work unit number(s). Use the following labels:

C	- Contract	PR	- Project
G	- Grant	TA	- Task
PE	- Program Element	WU	- Work Unit Accession No.

Block 6. Author(s). Name(s) of person(s) responsible for writing the report, performing the research, or credited with the content of the report. If editor or compiler, this should follow the name(s).

Block 7. Performing Organization Name(s) and Address(es). Self-explanatory.

Block 8. Performing Organization Report Number. Enter the unique alphanumeric report number(s) assigned by the organization performing the report.

Block 9. Sponsoring/Monitoring Agency Name(s) and Address(es). Self-explanatory.

Block 10. Sponsoring/Monitoring Agency Report Number. *(If known)*

Block 11. Supplementary Notes. Enter information not included elsewhere such as: Prepared in cooperation with....; Trans. of....; To be published in.... When a report is revised, include a statement whether the new report supersedes or supplements the older report.

Block 12a. Distribution/Availability Statement. Denotes public availability or limitations. Cite any availability to the public. Enter additional limitations or special markings in all capitals (e.g. NOFORN, REL, ITAR).

DOD - See DoDD 5230.24, "Distribution Statements on Technical Documents."
DOE - See authorities.
NASA - See Handbook NHB 2200.2.
NTIS - Leave blank.

Block 12b. Distribution Code.

DOD - Leave blank.
DOE - Enter DOE distribution categories from the Standard Distribution for Unclassified Scientific and Technical Reports.
NASA - Leave blank.
NTIS - Leave blank.

Block 13. Abstract. Include a brief *(Maximum 200 words)* factual summary of the most significant information contained in the report.

Block 14. Subject Terms. Keywords or phrases identifying major subjects in the report.

Block 15. Number of Pages. Enter the total number of pages.

Block 16. Price Code. Enter appropriate price code *(NTIS only)*.

Blocks 17. - 19. Security Classifications. Self-explanatory. Enter U.S. Security Classification in accordance with U.S. Security Regulations (i.e., UNCLASSIFIED). If form contains classified information, stamp classification on the top and bottom of the page.

Block 20. Limitation of Abstract. This block must be completed to assign a limitation to the abstract. Enter either UL (unlimited) or SAR (same as report). An entry in this block is necessary if the abstract is to be limited. If blank, the abstract is assumed to be unlimited.